1992

A kinematic model of baroclinic tidal currents at the head of Monterey Submarine Canyon

Andrew Justin Heard
San Jose State University

Order Number 1348686

A kinematic model of baroclinic tidal currents at the head of Monterey Submarine Canyon

Heard, Andrew Justin, M.S.

San Jose State University, 1992

U·M·I
300 N. Zeeb Rd.
Ann Arbor, MI 48106

A KINEMATIC MODEL OF BAROCLINIC TIDAL CURRENTS AT THE HEAD OF MONTEREY SUBMARINE CANYON

A Thesis

Presented to

The Faculty of Moss Landing Marine Laboratories

San Jose State University

In Partial Fulfillment

of the Requirements for the Degree

Master of Science

in

Marine Science

By

Andrew Justin Heard

May 1992

APPROVED FOR MOSS LANDING MARINE LABORATORIES

William Broenkow

Dr. William W. Broenkow

Kenneth S Johnson

Dr. Kenneth S. Johnson

Dr. Nicholas A. Welschmeyer

APPROVED FOR THE UNIVERSITY

Serena M. Stanford

ABSTRACT

A KINEMATIC MODEL OF BAROCLINIC TIDAL CURRENTS
AT THE HEAD OF MONTEREY SUBMARINE CANYON

by Andrew Justin Heard

Rectification of the internal tide near the Monterey Submarine Canyon head results in net transport of deep water out of the canyon. Harmonic regression of CTD time series showed the presence of 70 m internal tides. These observations are consistent with theoretical models of Hotchkiss and Wunsch (1982) and suggest that canyon geometry selectively focuses and amplifies the M_2 internal tide. Calculation of the volume divergence from changes in isopycnal spacing yield lateral bottom speeds of 4 cm/s across the canyon flanks.

Currents were measured using a vessel mounted Acoustical Doppler Current Profiler and were analyzed using harmonic least square regression. Oscillatory, two layer flow was observed, consistent with theoretical flow patterns of internal waves. Measured bottom amplitudes increased 5 cm/s over the canyon flank as a result of the baroclinic tide. Rectification of the baroclinic tide resulted in a mean up-canyon flow which produces an upward vertical velocity estimated to be 50 m/day. The volume of water pumped out of the canyon is 60% of the calculated volume divergence during an internal tidal cycle.

ACKNOWLEDGEMENTS

The accomplishment of this thesis would not have been possible without the help and support of many people. I am especially indebted to Dr. William Broenkow. Not only did he teach me oceanographic theory, but provided the practical experience and knowledge needed to apply it in the real world. During the writing of this thesis he has tolerated my lack of writing skills, and busy work schedule with humor and patience. His help during the final preparation of this thesis is especially appreciated.

Through Dr. John Martin's directorship, students, such as myself, have benefitted through state-supported research cruises aboard Pt. Sur. I would also like to thank Drs. Kenneth Johnson and Nicholas Welschmeyer for agreeing to serve on my committee. A special thanks goes to Gail Johnson for assistance with the paperwork necessary to graduate. Sheila Baldridge and Sandi O'Neil's help in the library is always appreciated. I would also like to thank Mike Prince for tolerating my lack of concentration while at work during the final months of completion of this thesis, and for allowing me time to work on it.

I would like to extend a special thanks to Paul Jessen at the Naval Postgraduate School. He provided the software and expertise to process the ADCP data. His advice and teachings were invaluable during the analysis of the data. Without his help much of this thesis would not have been possible.

I am lucky to have been surrounded by many wonderful friends while attending the Marine Lab. Mark Yarbrough helped me to understand much about being a technician, both at sea and ashore. The friendship of my cohorts, Marilyn Yuen, Cary and Claire Wong and Mark and Sandy Yarbrough is worth more than anything taught in classes. Their friendship and our experiences will last a lifetime.

I would finally like to thank my wife Janet. Her daily love and support are why this thesis was finished. Words cannot express how much her love means to me. She also performed much of the drafting for the final figures. In addition while I went to sea to work, she tied up many of the loose ends and coordinated many of the last minute details involved in finalizing a thesis. For all her help and support I am eternally grateful.

TABLE OF CONTENTS

LIST OF FIGURES

LIST OF TABLES

INTRODUCTION

Oceanography in coastal regions is extremely dynamic. The boundary between land and sea influences wind and current patterns, which in turn causes strong lateral gradients in oceanographic properties. Nearshore circulation is complicated by filamentous flow near capes, wind driven upwelling along the open coast, and estuarine circulation near rivers. In Monterey Bay, however, the presence of a large submarine canyon influences strongly, and in some ways dominates, circulation patterns within the Bay. Monterey Submarine Canyon (MSC), one of the largest in the world, compares in size to the Grand Canyon (Shepard and Dill, 1966). Originating near Moss Landing, California, the Canyon bisects Monterey Bay, and has a volume of 420 km^3 (Martin, 1964). At the outer edge of the Bay, MSC is roughly 12 km wide and 1000 m deep (Fig. 1).

Circulation in Monterey Bay is complex. A scale analysis done by Breaker and Broenkow (1989) suggest that within two orders of magnitude, all the terms in the horizontal equations of motion are approximately equal. The barotropic tide was most important, followed by the internal density field and the Coriolis force. This is very different from the offshore case for which the dominant terms are pressure and Coriolis. The result of this suggests that circulation in Monterey Bay may respond to a complex interaction of many processes.

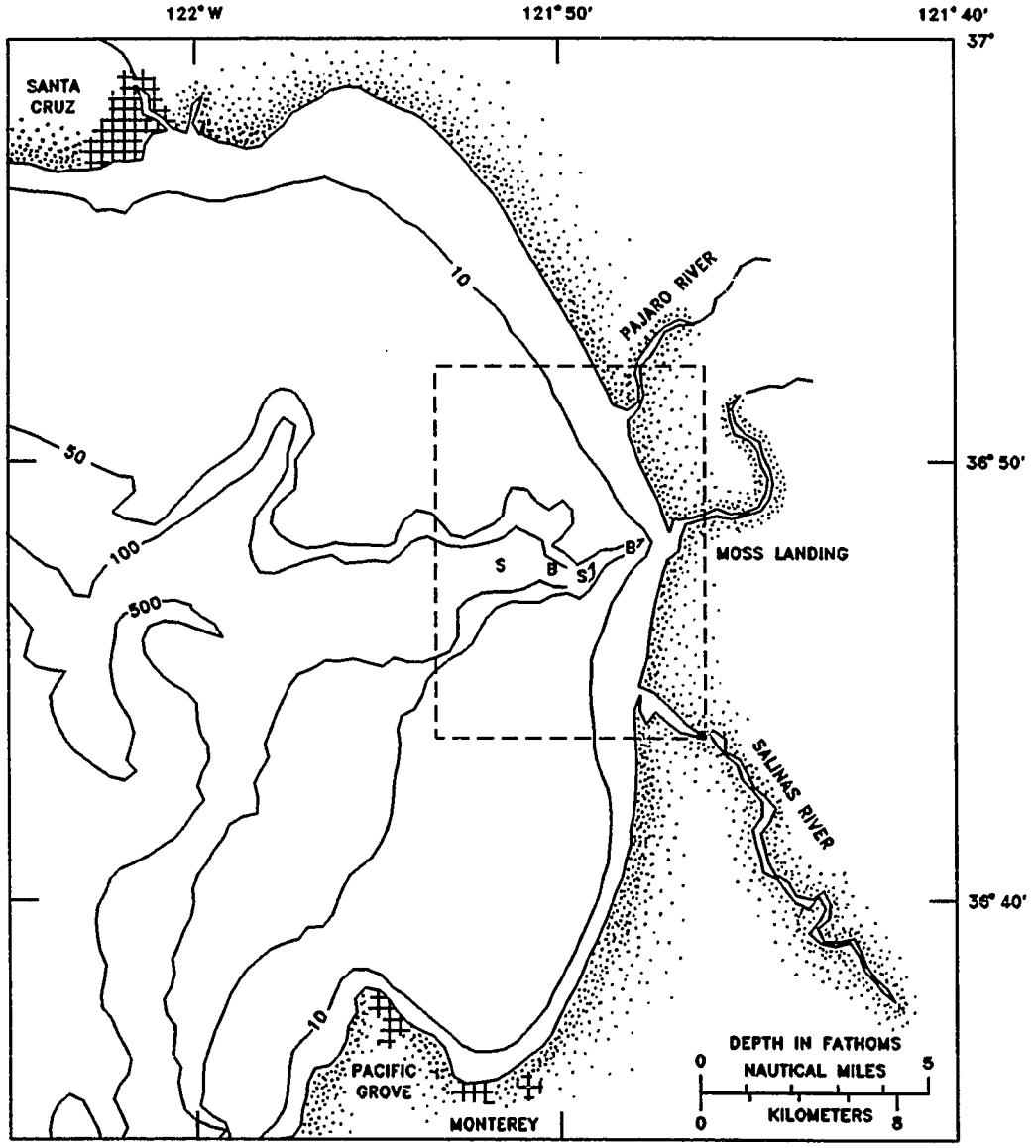

Figure 1. Area map of Monterey Bay showing locations of previous internal tide measurements. Measurements by Broenkow and McKain (1972) are shown by *B* and by Shea and Broenkow (1982) by *S*. The outlined area is shown in Fig. 2.

Knowledge of surface circulation in Monterey Bay is based on many measurement techniques. Currents are strongly tidal, with peak speeds on the order of 20 cm/s (Breaker and Broenkow, 1989). Mean flow is thought to be generally northward at about 5 cm/s. However, the currents episodically reverse direction and flow south about one-third of the time (Broenkow and Smethie, 1978).

Flow in the canyon is less well known. Early studies by Gatje and Pizinger (1965) and Dooley (1968) showed bottom currents near the Canyon head tend to follow the Canyon axis. Mean speeds were on the order of 10 to 12 cm/s with bursts as high as 60 cm/s. Shepard (1979) found a net up-canyon flow at several stations. In all these studies only one or two depths were sampled, usually within 30 m of the bottom. Thus, while the bottom currents have been studied, the remaining water column velocity structure remains relatively unknown.

In addition to currents, Dooley (1968) and Shepard (1979) noted internal waves of tidal periods in MSC. Broenkow and McKain (1972) and Shea and Broenkow (1982) specifically quantified the internal tide in greater detail. Measurements of internal waves in the open ocean are relatively rare. However, the presence of internal waves in submarine canyons is not uncommon (Hotchkiss and Wunsch, 1982).

Internal tides are thought to be generated by the advection of stratified water across the continental slope by the barotropic tide (Baines, 1986). Bumps on the bottom, and canyon slopes and walls, are though to be particularly good places to generate internal tides (Baines, 1973; Baines, 1983). Hotchkiss and Wunsch (1982) suggest that

internal tides generated in canyons can be reflected up the canyon by the bottom and walls. This will tend to concentrate the wave energy along the bottom and at the head of the canyon. Wunsch and Webb (1979) showed a large increase in the wave energy field from mouth to head in Hydrographer canyon, and Hotchkiss and Wunsch (1982) obtained similar results in Hudson canyon.

Large internal tides are present near the head of Monterey Canyon. Waves of 80 to 120 m have been reported by Broenkow and McKain (1972) and Shea and Broenkow (1982). These are some of the largest amplitudes ever found in the world's oceans. Broenkow and McKain calculated by conservation of volume that the change in isopycnal spacing during a falling tide required currents on the order of 9 cm/s over the flanks of the canyon at depths between 10 to 40 m. Shea and Broenkow (1982) obtained similar results. They found that low temperature, high density water spilled over the flanks of the canyon during a rising tide and spread laterally along the bottom. This lens of water was on the order of 20 m thick, and was estimated to affect directly an area 26 km^2. On the falling tide some of this water was pinched off and left behind. Shea and Broenkow (1982) suggest that this tidal pumping promoted a net upward movement of cold, nutrient rich deep water to the surface waters near the canyon. In addition, this process should affect the bottom currents on the shelf near the canyon.

Until the 1980's, current measurements were made with meters moored at discrete depths, by drifters and drogues, or by geostrophic or continuity calculations. Since then, a new current measurement

technology, the Acoustic Doppler Current Profiler (ADCP), has been developing. The ADCP uses range gated, Doppler shifted sound to provide a water column current velocity profile vs. depth. With a vessel mounted ADCP, continuous profiles of water column velocity can be obtained from a moving ship. In practice, this is not an easy process. The ADCP is a complicated instrument (some details are provided in the Appendix), and before quality data can be obtained, some effort must be directed toward understanding hardware and software, and patience is required during both data acquisition and processing.

The purpose of this study was to use a vessel-mounted ADCP to directly measure currents associated with internal tides in Monterey Submarine Canyon. Of primary interest was the measurement of increased bottom velocity over the flanks of the canyon postulated by Broenkow and McKain (1972) and Shea and Broenkow (1982). Other objectives were to make some of the first direct measurements of water column velocity structure within the canyon, and to further characterize the internal tides at the head of the canyon.

METHODS

This study was conducted in conjunction with regularly scheduled class cruises for the Moss Landing Marine Laboratory aboard the Research Vessel Point Sur. The study was made during one tidal day, starting at 10:00 local (+8) time on 14 March 1989. During this period the goal was to measure currents by ADCP over the center of the canyon during CTD casts used to characterize the internal tide and then to make vertical velocity profiles over the flanks of the canyon. To accomplish this, a transect loop was run roughly parallel to the isobaths (Fig. 2). The starting point, Station 1, was positioned over the canyon axis at 36° 47.8'N, 121° 49.3'W at a depth of 185 m. The transect proceeded northward 2.5 miles to Position 2, the ship turned, ran south 5 miles through Station 1, to Position 3, turned and returned to Station 1. Transects were run at 10 kts. During the cruise, we later decided to make ADCP measurements while sitting at a station for 30 min. This was done partially to compare ADCP data obtained at Station 1 while making CTD profiles, and to allow CTD sampling over the flanks of the canyon. Two new stations were established, Station 5, 0.5 miles north of the canyon and Station 4, 1 mile south of the canyon (Table 1).

The ADCP was configured to acquire data in 2 min ensembles and 4 m depth bins. At 10 knots the 2 min ensembles yielded a horizontal bin distance of 600 m. The velocity measurement error stated by the manufacturer for this configuration was 3 cm/s. Bottom tracking was

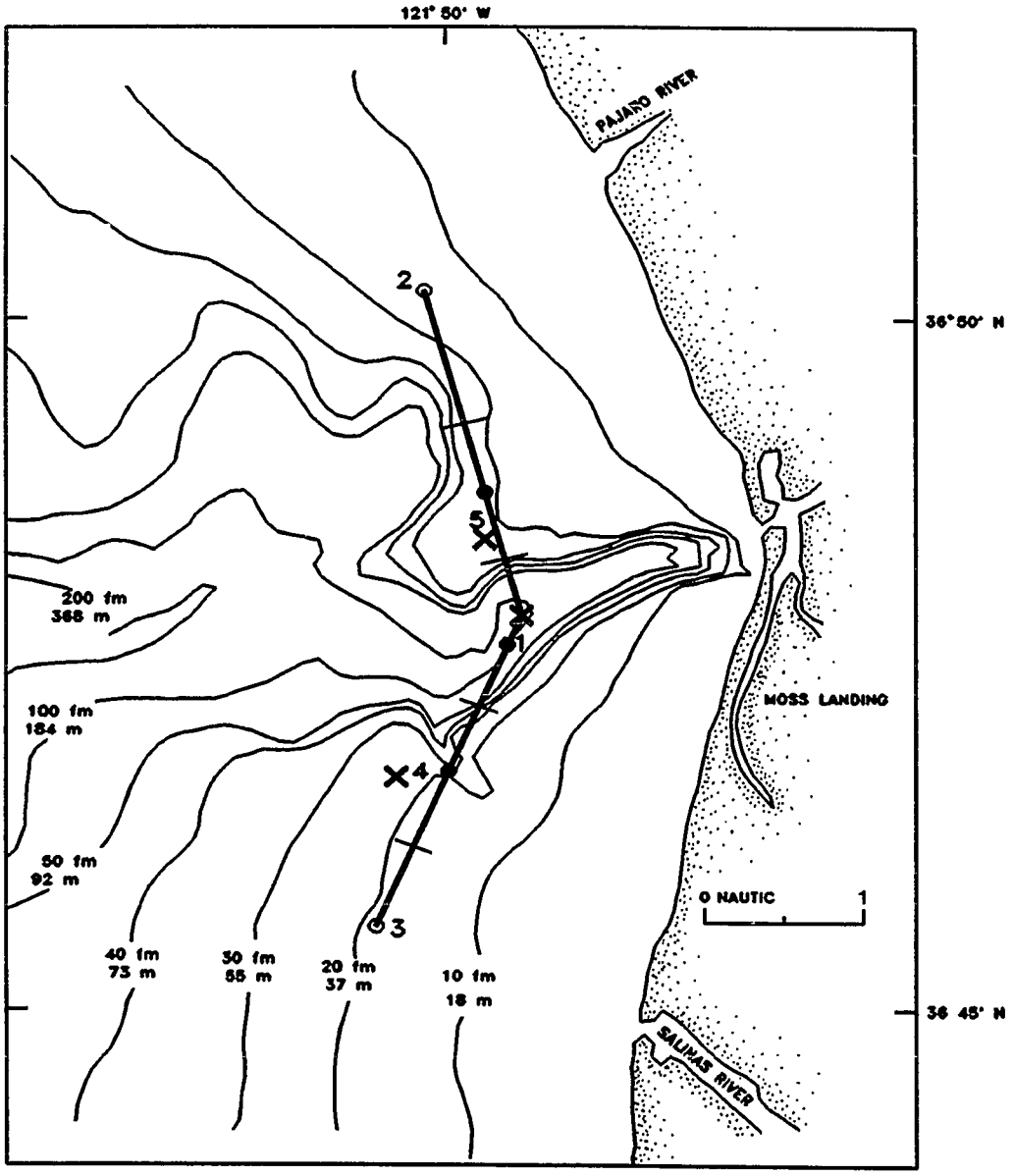

Figure 2. ADCP transect line and CTD positions, 14-15 March, 1989. Station locations are given in Table 1. The ADCP transect was run from 1-2-1-3-1. CTD stations are shown by the X. The spatially averaged ADCP stations 1,4,5 are filled circles. Horizontal bars on the transect line show the limits over which ADCP stations 1,4,5 were averaged.

Table 1. Positions and depths of stations occupied during the study.

Station	North Latitude	West Longitude	Depth (m)
1 ADCP	33° 47.7′	121° 49.4′	185
2 ADCP	36° 50.2′	121° 50.2′	30
3 ADCP	36° 45.5′	121° 50.3′	33
4 ADCP	36° 46.6′	121° 49.9′	38
5 ADCP	36° 48.5′	121° 49.6′	42
1 CTD	36° 47.8′	121° 49.3′	185
4 CTD	36° 46.6′	121° 50.3′	45
5 CTD	36° 48.3′	121° 49.6′	45

used throughout the cruise to correct for ship speed, and ship's position was also obtained from a Trimble 10x LORAN receiver, which allowed two separate estimates of ship velocity for data processing.

CTD profiles were obtained using a Seabird SBE-9 CTD. Data were sampled at 24 hz, and averaged to 1 s intervals. Salinity, depth and density were calculated from the conductivity, temperature and pressure measurements from the CTD using SeaBird software. Casts were made approximately every 1.5 hr at Station 1, over the canyon. Occasional casts were also made at Stations 4 and 5. Density data were interpolated to a 5 m by 1 hr grid and contoured.

ADCP data were processed using software provided by Paul Jesson at the Naval Postgraduate School. An early version of the software was used soon after the cruise to convert the raw binary files to ASCII text files for analysis by the MS-202 class. This version of the software did not extract bottom tracking data, but used LORAN positions to determine ship's motion. When the data were reanalyzed with a newer version of the software that would read the bottom tracking, it was found that the original disk was corrupted and no longer readable. This resulted in the loss of bottom tracking data for the first eight hours of the study. The entire data set was corrected using LORAN as a ship's motion reference and the last 18 hours was also processed using bottom tracking.

Data processing consisted of several steps. First the raw binary files were converted to ASCII text files and position and bottom tracking data extracted into separate files. The position data, or

bottom tracking data, were then used to calculate ship's velocity. An absolute velocity reference layer was created from the raw velocities and the ship's velocity. This reference layer was then filtered using a Hamming window with a cut-off frequency of 0.04 cycles /min (T = 25 min). The filtered reference layer was then used to correct the remainder of the velocity profile.

Data were then spatially and temporally averaged into three ADCP stations, which were centered around the three CTD Stations, Station 5, 1, and 4. Each ADCP station consisted of one transect or stationary sampling period. These stations did not include the end points of the transects where the data were contaminated from rapidly changing ship's motions during turns. Averaging by stations also allowed comparison of transect data with data taken during stationary CTD or ADCP sampling. Each average was edited individually to remove obviously bad ensembles. These commonly occurred when the ship started, stopped or changed direction. The same ensembles were deleted from both the navigation corrected files and the bottom tracking files to allow a comparison of the two methods.

It is important to recognize that much of the work in obtaining good velocity measurements occurs during post processing of the data. This is a tedious process, often taking days to process a 24 hr current record. Interpretation of ADCP data and comparison of ADCP results with those from traditional current meters are both difficult. Current meters produce a record of velocity at one point in space over a long time period, while vessel mounted ADCPs produce velocity records at many

time intervals and many depth or distance bins. The two data sets are not often comparable.

Data averaging, while necessary to improve accuracy and make data comparable also led to a much reduced data set. Since it is impossible to be in three places simultaneously, large gaps were present in the time series at each station. To better estimate the velocity structure at the three stations, least-squares harmonic regressions were performed on the current speeds at all depths, using both the M_2 and K_1 tidal constituent periods. These are the dominant semi-diurnal and diurnal periods of the surface tides in Monterey Bay reaching amplitudes of 1.628 and 1.211 feet, respectively. The regression equation is of the form:

$$X = A_0 + A_{M_2}\cos\left(\frac{t}{M_2}+L_{M_2}\right) + A_{K_1}\cos\left(\frac{t}{K_1}+L_{K_1}\right), \qquad 1$$

where X is the measured speeds or wave heights, A the calculated amplitudes for the regressed constituents, L the calculated phase lags for these constituents, M_2, K_1 are the speed numbers for these constituents (28.98 and 15.04 deg/hr), and t is time. To relate phasing between currents, the internal, and the surface tides, regressions were also performed on the time varying depth of various isopycnal surfaces, as well as the predicted surface tidal height.

RESULTS

The predicted tidal cycle for the study period (Fig. 3) shows a mixed semidiurnal type as is typical in Monterey Bay and along the northeast Pacific. The maximum change was 5.5 ft from higher high water at 04:30 to lower low water at 13:00. The rising tides resulted in a change of 3.6 ft for the first rising tide and 2.2 ft for the second. The two rising tides were separated by a falling tide of only 2.2 ft lasting for three hours.

While the surface tide was mixed, the internal tide (Fig. 4) displayed a predominantly semi-diurnal period. The crests were slightly trochoidal, as is typical of waves entering shallow water. The 26.0 sigma-t surface showed a vertical displacement of 54 m and the 26.25 sigma-t surface showed a displacement of 75 m. Harmonic regression on time varying depth of the isopycnal surfaces (Table 2) revealed the largest amplitude occurred at the 26.25 sigma-t surface. This surface was centered at 60 m with an amplitude of 29 m for the M_2 constituent and 10 m for the K_1. The M_2 constituent amplitudes for all isopycnals were 2 to 3 times greater than the K_1 amplitudes. The M_2 constituent of the internal tide lagged the M_2 constituent of the surface tide by 2.3 hr (70°), and the K_1 internal constituent preceded the K_1 surface tide by 1.7 hours. The deeper isopycnals lagged the shallower ones at both the M_2 and K_1 periods. This lag was on the order of 0.5 hr for the M_2 constituent and 1.5 hr for the K_1.

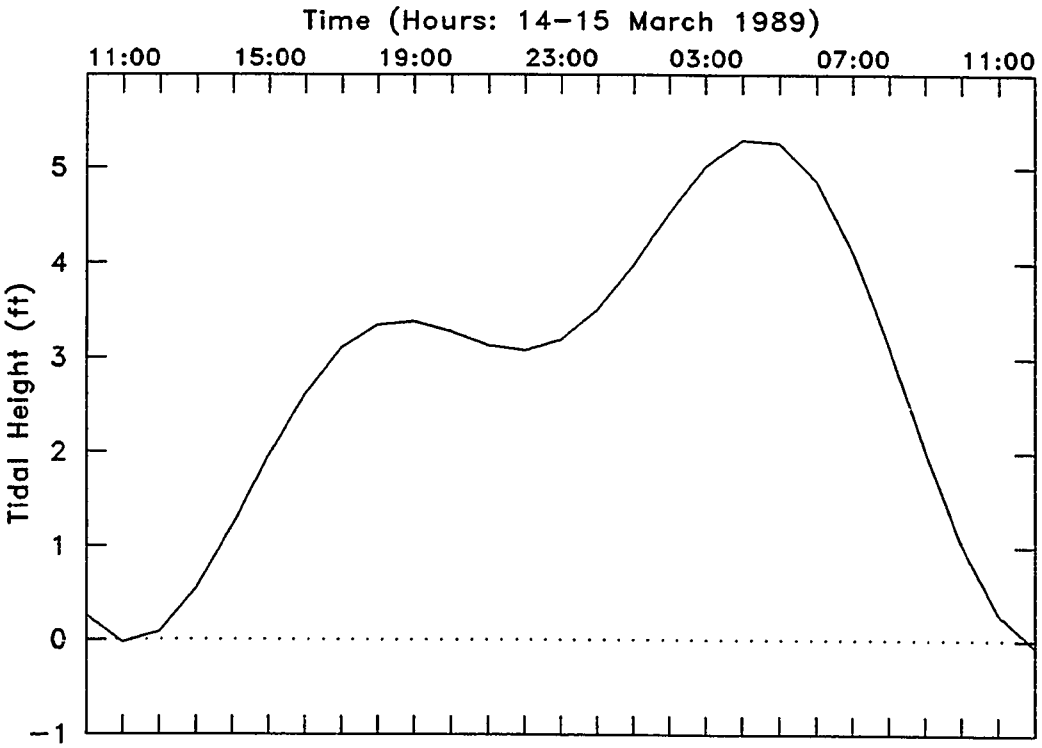

Figure 3. Predicted surface tidal height in feet for Monterey, California during the study period. Time starts at 10:00 on 14 March 1989 and ends at 12:00 on 15 March 1989. Times are local (+8).

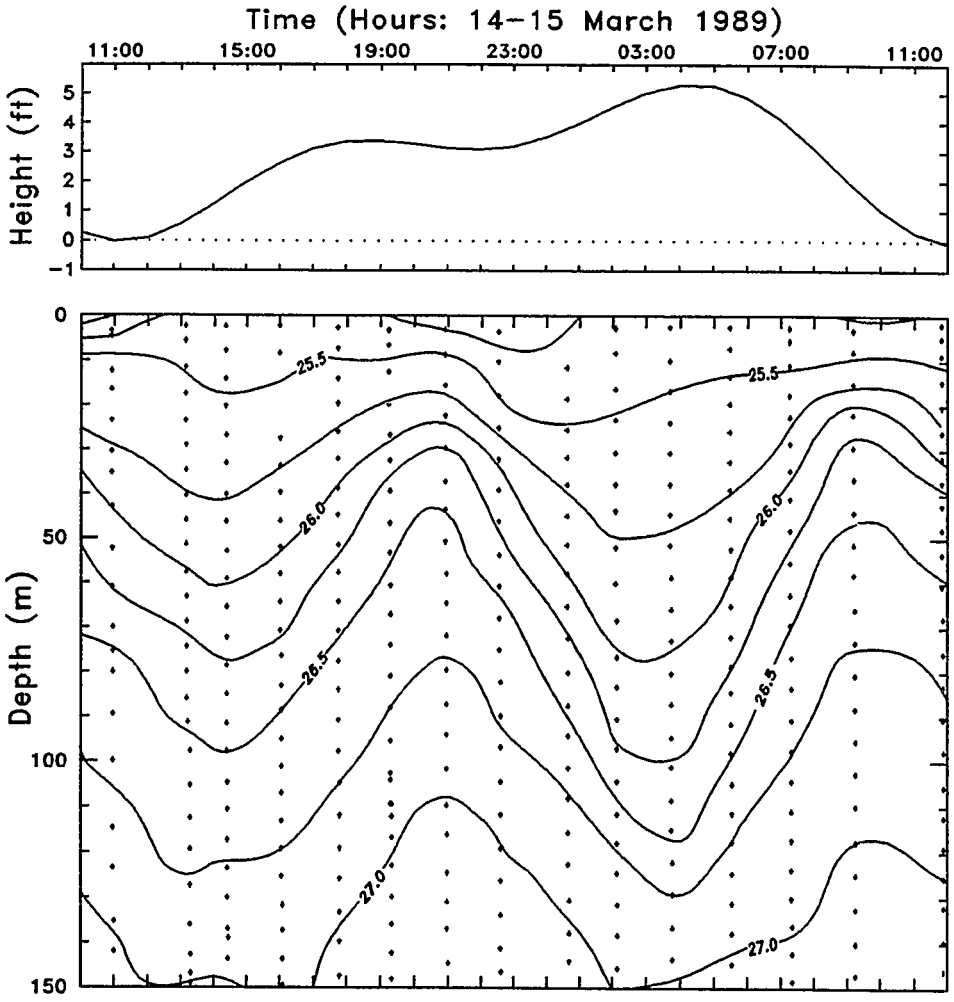

Figure 4. Distribution of sigma-t at Station 1 between 10:00 (+8) 14 March, 1989 and 12:00 (+8) 15 March 1989 showing the presence of a large internal tide of approximately 12 hr period (lower panel). Contour interval is 0.25 sigma-t. Bottom depth at Station 1 is 185 m. Upper panel shows predicted surface tidal height from Fig. 3 for comparison.

Table 2. Coefficients from the harmonic regressions of the time varying depth of isopycnal surfaces and the predicted surface tidal height at the M_2 and K_1 periods. The regression equation is give by Eq. 1. Coefficients are the amplitudes in meters for the specific period. L is the phase lag in degrees relative to 10:00 (+8) 14 March 1989. F is the computed variance ratio. S_A is the standard error of the amplitude, in meters, and S_{yx} is the standard error of the estimate. Critical value of the F ratio at the 0.05 level is 4.2.

Surface	A_0	A_{M2}	L_{M2}	F_{M2}	A_{K1}	L_{K1}	F_{K1}	S_A	S_{yx}	R	N
Predicted tide	0.9	0.4	204	1225	0.6	232	2388	0.01	0.03	0.99	27
σ_t=25.50	14	5	97	17	4	226	15	1	3	0.87	27
σ_t=25.75	31	14	126	386	5	257	47	1	2	0.99	27
σ_t=26.00	46	23	131	512	8	256	56	1	3	0.99	27
σ_t=26.25	60	29	134	248	10	263	28	2	5	0.98	27
σ_t=26.50	78	29	136	201	9	276	17	2	5	0.98	27
σ_t=26.75	103	24	138	75	1	280	0.2	3	7	0.93	27
σ_t=27.00	135	18	144	92	5	004	8	2	5	0.95	27

The currents showed periodicity consistent with tidally induced flow. Flow was aligned more or less parallel to the isobaths (Fig. 5), being predominantly east-west at Station 1 and inclined northeast-southwest at Stations 4 and 5. Surface speeds were on the order of 20 to 30 cm/s. Results from the harmonic regressions are shown in Figs. 6 and 7 and Table 3. Consistent with usual oceanographic notation, positive u component velocities are to the east and positive v component velocities are to the north. The daily-mean flow was to the south at all stations. The north-south mean flow was larger than the east-west flow. At Station 5, the mean northerly speed was -5 cm/s while the easterly component was 2 cm/s. At Station 1, over the canyon, the surface flow was aligned closely with the canyon axis. There the mean u component velocity was 3 cm/s and the v component was -1 cm/s. At Station 4, the mean u component was -4 cm/s and the v was -4 cm/s. The change in sign of the u component between Station 4 and 5 indicates that the southerly flow is steered by the bathymetry around the canyon.

The surface current amplitudes from the harmonic regression analysis were also larger in the north-south direction than east-west (Fig. 6 and 7). The M_2 constituent amplitudes were on the order of 10 cm/s for the v component and 7 cm/s for the u component. The statistical limits for the amplitude estimates were 2 to 3 cm/s. The K_1 v component showed similar results. Both constituent v component amplitudes were 3 to 4 cm/s faster at the flank stations (4 and 5) than

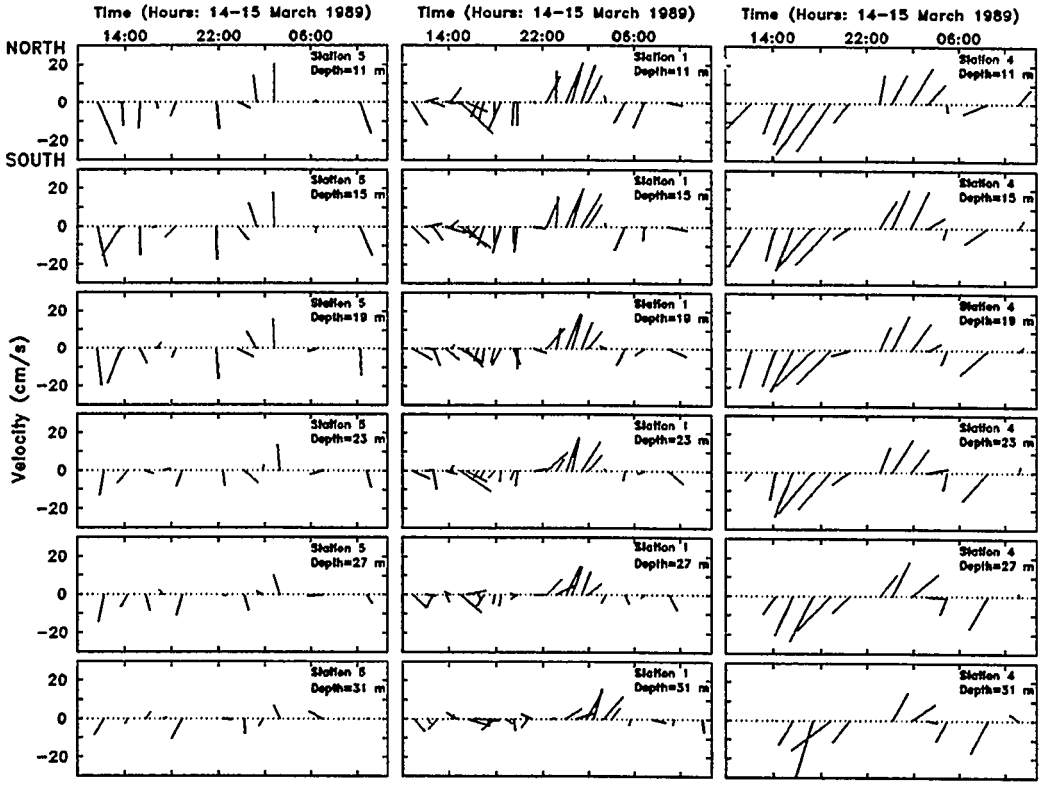

Figure 5. Stick diagrams of spatially and temporally averaged ADCP measured currents showing the tidal nature of the flow. Station 5,1,4 locations are shown in Fig. 2. Labeled depths are the center of each 4 m ADCP bin. Northward flow is towards the top of the figures, as shown for Station 5 at 11 m.

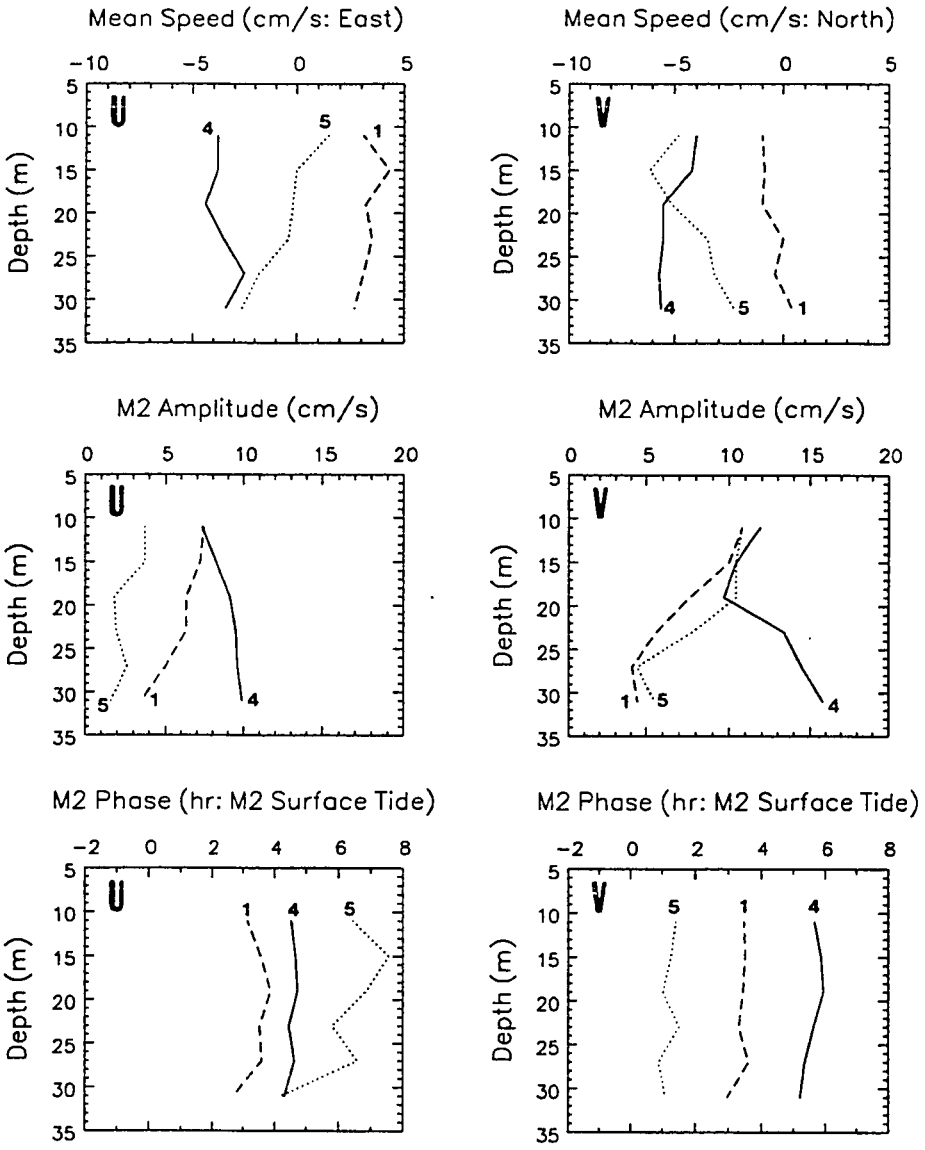

Figure 6. M_2 period harmonic regression coefficients from currents shown in Fig. 5. U component velocities are on the left and V velocities are on the right. Station numbers are shown near each line. The increase in v component amplitude over the last 10 m at Station 4 is consistent with increased bottom speeds caused by the internal tide. Phasing is shown relative to the time of maximum M_2 constituent surface tidal height. Positive hours indicate that maximum currents occur after maximum tidal height.

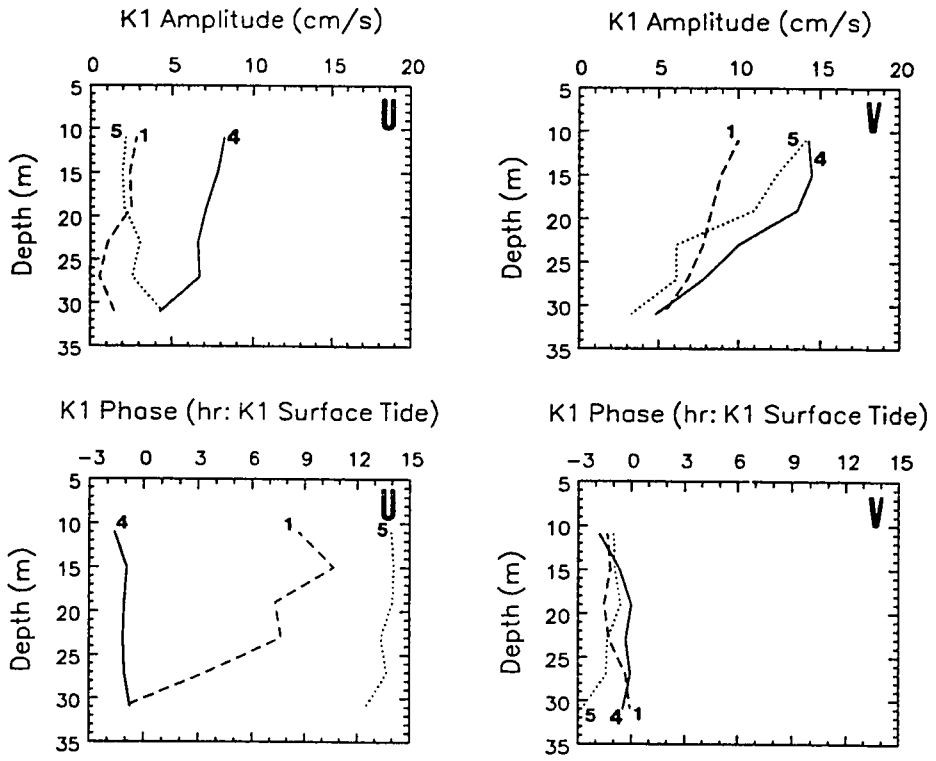

Figure 7. K_1 period harmonic regression coefficients for currents shown in Fig. 5. Left side panels are for the u component and right side panels are the v component. Station numbers are shown near each line. Mean flows are shown in Fig. 6. Phasing is shown relative to the time of maximum K_1 constituent surface tidal height. Positive hours indicate that maximum currents occur after maximum tidal height.

Table 3. Coefficients from the harmonic regressions of u and v component current velocity in Fig. 5 at the M_2 and K_1 periods. Coefficients are described in Table 2. Amplitudes are in cm/s and phases in deg relative to 10:00 (+8) 14 March 1989. The critical value of the F ratio at the 0.05 level for Station 5 is 6.0 (6.6 at 31 m); at Station 1 is 4.7; at Station 4 is 5.3 (5.6 at 27 m and 6.6 at 31 m).

Depth	A_0	A_{M2}	L_{M2}	F_{M2}	A_{K1}	L_{K1}	F_{K1}	S_A	S_{yx}	R	N
					Station 5 u component						
11	1.5	3.7	17	5.0	2.17	22	1.6	1.6	2.65	0.83	11
15	0.0	3.7	-15	1.5	2.03	20	0.4	3.0	4.81	0.63	11
19	-0.2	1.8	5	0.3	2.11	21	0.4	3.3	5.04	0.40	11
23	-0.4	1.9	36	0.4	3.06	31	1.2	2.8	4.33	0.56	11
27	-1.8	2.6	13	1.8	2.56	26	1.7	1.9	3.09	0.69	9
31	-2.6	1.6	82	0.4	4.44	44	3.0	2.4	3.52	0.72	9
					Station 5 v component						
11	-4.8	10.8	163	11.1	14.1	247	18.1	3.3	5.2	0.95	11
15	-6.1	10.4	167	5.4	12.3	246	7.4	4.5	7.2	0.89	11
19	-5.1	10.4	174	6.8	11.0	241	7.3	4.1	6.4	0.90	11
23	-3.5	7.8	160	8.9	6.1	252	5.2	2.6	4.2	0.90	11
27	-3.2	4.4	178	1.3	6.1	253	2.4	3.8	6.1	0.73	9
31	-2.3	5.5	172	1.6	3.3	-86	0.9	3.6	5.7	0.68	9
					Station 1 u component						
11	3.1	7.4	113	13.6	2.8	102	1.9	2.0	4.2	0.82	18
15	4.3	7.2	101	11.6	2.4	72	1.2	2.1	4.4	0.80	18
19	3.2	6.3	92	12.1	2.5	122	1.7	1.8	3.8	0.81	18
23	3.5	6.3	102	8.0	1.1	117	0.2	2.2	4.6	0.74	18
27	3.1	5.0	100	9.0	0.6	180	0.1	1.7	3.4	0.77	18
31	2.7	3.5	126	3.0	1.5	249	0.6	2.0	4.1	0.64	18

Table 3. (continued)

Depth	A_0	A_{M2}	L_{M2}	F_{M2}	A_{K1}	L_{K1}	F_{K1}	S_A	S_{yx}	R	N
					Station 1 v component						
11	-1.0	10.8	103	24.5	10.0	252	20.8	2.2	4.5	0.95	18
15	-0.9	10.0	102	25.7	8.9	250	20.2	2.0	4.1	0.95	18
19	-1.0	7.6	104	18.7	8.3	255	21.8	1.7	3.7	0.95	18
23	0.0	5.6	108	7.8	7.8	251	14.7	2.0	4.2	0.91	18
27	-0.4	4.1	99	4.2	6.8	237	11.8	2.0	4.0	0.88	18
31	0.4	4.4	118	5.5	5.3	233	7.7	1.9	3.9	0.85	18
					Station 4 u component						
11	-3.8	7.3	73	4.4	8.2	256	5.9	3.3	5.9	0.88	13
15	-3.8	8.2	69	8.8	7.8	246	8.3	2.6	4.8	0.92	13
19	-4.4	9.1	67	21.3	7.1	248	13.4	2.0	3.4	0.95	13
23	-3.5	9.5	75	32.8	6.6	249	16.4	1.7	2.9	0.97	13
27	-2.5	9.6	70	35.5	6.7	248	18.9	1.4	2.6	0.98	12
31	-3.4	9.9	79	12.0	4.3	243	2.7	2.6	3.8	0.96	10
					Station 4 v component						
11	-4.0	11.9	40	15.3	14.3	259	22.5	3.2	5.3	0.96	13
15	-4.2	10.4	34	9.6	14.5	242	18.6	3.3	5.9	0.95	13
19	-5.5	9.7	32	9.5	13.6	232	18.4	3.3	5.5	0.95	13
23	-5.5	13.4	41	75.3	10.0	237	41.6	1.4	2.7	0.99	13
27	-5.7	14.5	49	99.2	7.8	233	28.7	1.3	2.4	0.99	12
31	-5.6	15.8	53	20.2	4.8	239	1.9	3.4	4.9	0.96	10

over the canyon. This is probably due to the bathymetric effects of the canyon, which runs in a more east-west direction, at Station 1. At Stations 4 and 5 the bathymetry runs north and south.

Phase lags from the harmonic regressions for the surface currents in the v direction showed that the variation in M_2 phase lag between the Stations is highly regular. The change progresses from north to south, with a phase lag of 2.1 hours between stations (Figs. 6 and 7). Maximum currents at Station 5 also lagged the maximum height of the M_2 component of the surface tide by 1.4 hours. For the K_1 constituent the progression of the phase lag was in the opposite direction. The time of maximum current speeds at Station 4 preceded the maximum height of the K_1 surface tidal constituent by 1.8 hours. Maximum speeds at Station 1 were 0.5 hours later than at Station 4, and maximum speeds at Station 5 occurred 0.3 hours after Station 1.

Since the current speed varied with depth the current profiles at all three stations showed evidence of baroclinicity (Fig. 5). However, because of the lack of data, it is hard to make many conclusions. Speeds at 31 m at Station 4 were larger than at the same depth at Station 1 or 5. Results from the harmonic regressions (Fig. 6 and 7) support this. For Station 5 the regression coefficients and subsequent F values were such that at the 0.05 level the regression coefficients were not significantly differently from random. This may be due to a small sample size. Significant regression coefficients for the M_2 period were obtained at Stations 1 and 4. At Station 4, the amplitude increased from 10 cm/s at 19 m to 16 cm/s at 31 m in the v direction and

by 1 cm/s in the u direction. Over the same depth range at Station 1 the speeds decreased by 3 cm/s in both components. Phasing was not depth dependent at any of the shallow stations. Note, however, that at Station 1 the bottom depth is much greater than at the shelf stations. For this portion of the analysis, only data down to 31 m at Station 1 were used to be consistent with the other stations.

The current profile for the full depth range at Station 1 in the canyon is presented in Fig. 8. Because currents at Station 1 were aligned with the canyon axis, data at Station 1 have been rotated 30 degrees and results are described in terms of along-canyon and cross-canyon currents. Positive values indicate flow up the canyon. The maximum depth for which ADCP data were obtained was 123 m, which is 60 m above the bottom. Flow in the canyon showed a definite two layer structure with the lower layer moving in the opposite direction of the surface layer. The whole water column showed periodic direction reversals approximately every 6 hours.

Harmonic regressions of data at Station 1 (Fig. 9; Table 4) showed significant correlation only at the M_2 period. The mean flow was up-canyon at all depths, with the surface speeds on the order of 1 cm/s and a maximum speed of over 7 cm/s at 119 m. The amplitudes and phasing showed the two layer flow clearly. The amplitude was 13 cm/s at the surface and decreased to a minimum of 2 cm/s at around 50 m. The amplitude increased again to a maximum of 7.6 cm/s at 119 m. The

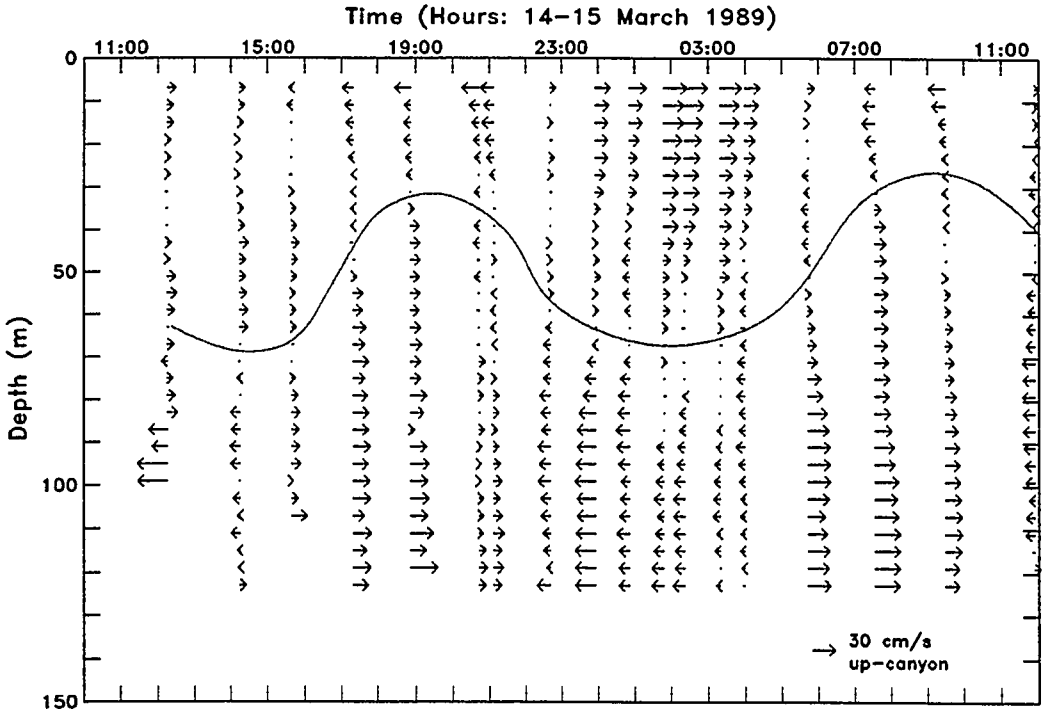

Figure 8. Along-canyon velocity profiles at Station 1 from 10:00 (+8) 14 March to 12:00 (+8) 15 March 1989 as measured by the ADCP. The bottom depth is 185 m, 60 m below the deepest currents measured. Maximum velocities are on the order of 30 cm/s. Flow to the right is up-canyon. Note the two layer flow consistent with theoretical velocity structure associated with internal waves. The depth of estimated current reversal is depicted by the illustrated wave.

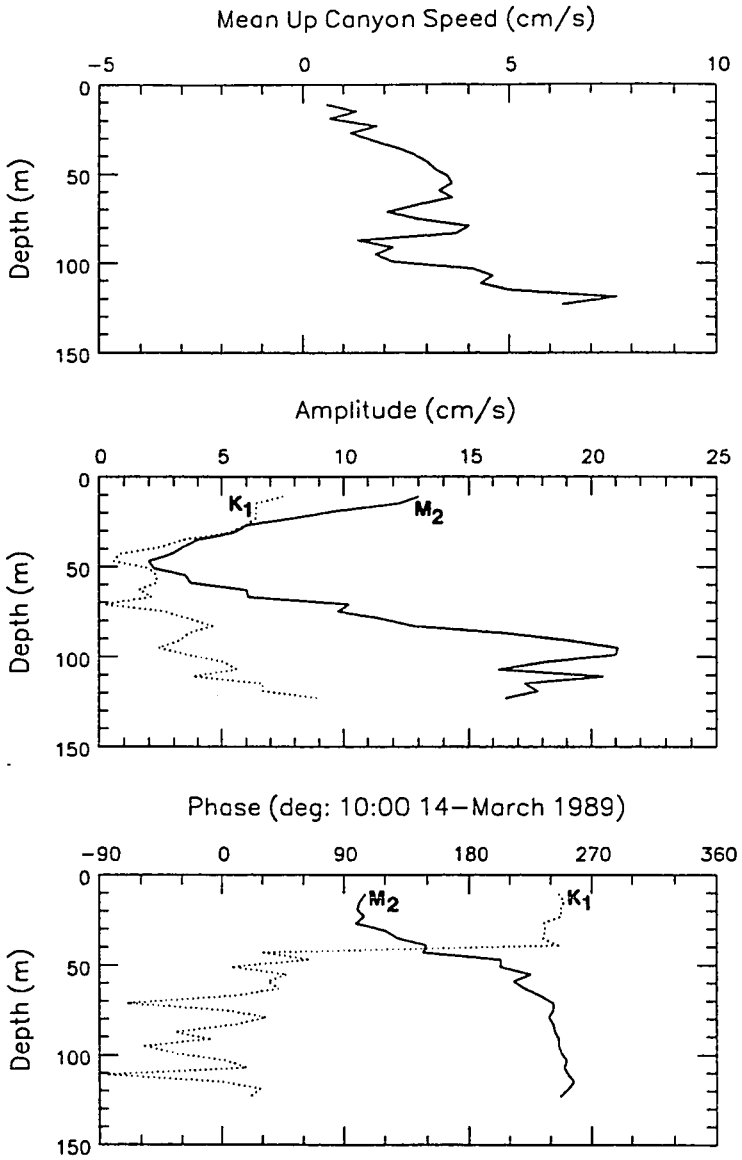

Figure 9. Harmonic regression results for the velocity profiles shown in Fig. 8. M_2 coefficients are shown by the solid line and K_1 coefficients by the dotted line. The mean flows are up-canyon at all depths. Two-layer flow is shown clearly by the amplitude and phase. Notice that the M_2 amplitudes are 2-3 times the K_1. Phasing is in degrees relative to 10:00 (+8) 14 March 1989 for both constituents.

Table 4. Coefficients from harmonic regression of along canyon flow shown in Fig. 8. Amplitudes are in cm/s and phases in deg relative to 10:00 (+8) 14 March 1989. The critical value of the F ratio at the 0.05 level is 4.7 (5.1 at 123 m).

Depth	A_0	A_{M2}	L_{M2}	F_{M2}	A_{K1}	L_{K1}	F_{K1}	S_A	S_{yx}	R	N
11	0.6	13.0	106	57.4	7.5	246	19.0	1.7	3.6	0.97	18
15	1.3	12.2	102	52.3	6.4	250	14.5	1.7	3.5	0.96	18
19	0.7	9.7	100	39.1	6.4	247	16.6	1.5	3.2	0.96	18
23	1.8	8.0	105	25.5	6.4	248	16.6	1.5	3.3	0.94	18
27	1.2	6.0	99	13.7	6.0	235	13.6	1.7	3.4	0.92	18
31	1.7	5.5	120	9.1	5.3	236	8.2	1.5	3.8	0.88	18
35	2.3	4.0	129	2.9	3.4	234	2.1	1.7	4.8	0.71	18
39	2.7	3.4	149	1.3	2.5	245	0.7	2.8	5.6	0.53	18
43	3.0	2.9	147	0.9	0.8	031	0.1	2.8	6.3	0.38	18
47	3.2	2.0	203	0.5	0.6	065	0.1	2.6	5.5	0.29	18
51	3.5	2.2	203	0.6	2.0	007	0.1	2.6	5.7	0.41	18
55	3.6	3.5	225	1.3	2.3	048	0.6	2.6	6.0	0.51	18
59	3.3	3.7	213	2.0	2.3	034	0.7	2.6	5.4	0.57	18
63	3.6	6.0	221	5.4	1.6	042	0.4	2.5	5.3	0.70	18
67	2.8	6.1	232	5.5	2.1	010	0.6	2.5	5.3	0.71	18
71	2.1	10.2	242	15.3	0.2	291	0.1	2.5	5.4	0.83	18
75	2.8	9.8	242	12.0	2.6	003	0.8	2.7	5.8	0.82	18
79	4.0	11.5	239	11.8	3.6	033	1.0	3.7	6.9	0.83	18
83	3.7	12.8	242	12.2	4.6	010	1.5	3.7	7.6	0.83	18
87	1.4	16.5	243	26.1	3.6	325	1.2	3.2	6.7	0.89	18
91	2.2	19.0	246	47.9	3.3	350	1.4	2.9	5.6	0.94	18
95	1.8	21.1	246	34.9	2.4	303	0.4	3.5	7.3	0.92	18
99	2.2	21.0	248	31.4	3.6	324	0.9	3.6	7.6	0.91	18
103	4.1	18.1	525	68.0	5.1	004	5.2	2.1	4.2	0.96	17
107	4.6	16.3	250	29.7	5.6	018	3.3	3.6	5.8	0.93	17
111	4.3	20.5	253	64.1	3.8	275	2.0	2.5	4.8	0.97	16
115	5.0	17.3	257	56.9	6.7	001	8.3	2.4	4.3	0.97	16
119	7.6	17.8	253	46.0	6.7	028	6.1	2.5	5.0	0.96	16
123	6.3	16.5	247	30.6	9.0	021	7.5	2.2	4.0	0.93	14

phasing showed the direction reversal occurred near 50 m where the amplitude was a minimum. The difference in phase between the layers was on the order of 150 degrees which may suggest the recurrence of some cross channel flow. The change in flow direction in the surface layer lagged the internal tide by approximately 1 hour and the surface tide by 3.4 hours. This suggests that the periodic flow pattern in the canyon during this study was primarily caused by the internal tide with a predominantly M_2 period.

DISCUSSION

ADCP Performance

An important objective of this study was to evaluate the operation and performance of the ADCP. Overall the ADCP performed well; however, two major problems emerged. One was with ship accelerations, which made estimating ship's velocity more difficult. This commonly occurred when the ship started, stopped, or changed course rapidly. The middle of the ADCP transect contained a course change of 35 degrees. While the course change allowed the ship track to parallel the bathymetry on both sides of the canyon, it also led to low data quality over the center of the canyon. Newer firmware and bottom tracking algorithms will help to reduce this type or error. However, best quality ADCP data can be obtained only when ship's accelerations are minimized.

The RMS difference in calculated speed between bottom tracking and LORAN navigation was about 4 cm/s (Table 5). This is consistent with calculated precision for LORAN-determined ship's speed of 2 to 4 cm/s (RDI 1989). However, RDI states their precision in terms of a single ensemble, whereas data reported here consist of several ensembles averaged together. Since averaging several ensembles should reduce errors, it is clear that the two methods of calculating ship's velocity did not lead to the precision suggested by RDI. New firmware received following completion of this study and a better understanding of the ADCP make it possible to realize field measurements closer to the manufacturer's stated precision.

Table 5. Comparison between ADCP currents calculated using bottom tracking and LORAN to calculate ship's motion. N and B subscripts refer to navigation (LORAN) and bottom tracking corrected u and v components. Velocities are from Station 1 at 15 m. Averages with high velocity differences were removed from the final records used for the harmonic regressions.

	u_n (cm/s)	u_b (cm/s)	abs(u_n-u_b) (cm/s)	v_n (cm/s)	v_b (cm/s)	abs(v_n-v_b) (cm/s)
	0.2	0.3	0.1	-17.1	-17.5	0.4
	-0.4	5.5	5.9	-4.9	-7.4	2.6
	-4.9	-4.2	0.8	11.8	12.2	0.4
	-3.7	-0.4	3.3	18.0	17.9	0.1
	0.2	-0.4	0.6	7.5	-3.1	10.6
	5.6	6.2	0.6	-13.9	-15.2	1.3
	-3.4	0.3	3.7	0.6	-8.9	9.6
	-2.6	-2.2	0.4	-15.3	-13.3	2.0
	5.5	6.9	1.3	0.5	-1.2	1.8
	3.2	6.4	3.2	19.0	12.7	6.3
	3.1	1.1	1.9	13.5	15.8	2.3
	13.2	10.6	2.6	23.4	19.6	3.8
	7.6	6.4	1.3	17.7	18.9	1.2
	14.7	11.4	3.3	19.5	17.2	2.3
	8.4	8.2	0.2	12.5	11.4	1.1
	-0.6	-0.3	0.2	-1.4	1.8	3.2
	-5.8	-5.5	0.3	-12.5	-12.6	0.1
	-3.9	-0.7	3.2	-8.2	-7.4	0.8
	10.5	11.2	0.7	1.6	-2.3	3.8
	-10.2	-7.8	2.4	-6.8	-5.5	1.2
	11.3	8.8	2.6	18.1	14.3	3.9
	-1.4	9.2	10.6	11.3	19.9	8.6
	0.1	9.3	9.2	14.7	19.4	4.7
	2.2	8.6	6.4	3.0	5.4	2.4
	-2.2	-1.6	0.6	-5.9	-5.2	0.7
	-10.4	-12.2	1.8	-6.4	-8.2	1.8
	-0.3	2.6	2.9	1.6	4.1	2.5
Mean	0.13	0.29	2.59	0.38	0.31	2.94
Std Dev	0.64	0.61	2.63	1.19	1.22	2.77
Min	-1.04	-1.22	0.10	-1.71	-1.75	0.09
Max	1.47	1.14	10.55	2.34	1.99	10.62
RMSE			3.69			4.04

The other problem with the ADCP operations as applied to this study was caused by side lobe interaction of the acoustic signal with the bottom. Since no acoustic transducer is perfectly focused directionally, weaker side lobe signals are generated outside of the main sound cone. The transducers are aligned at 30 degrees from the vertical to allow vector components to be calculated from the radial doppler shifted echos along the transducer axis. However, this angle also directs one of the side lobes toward the bottom. The strong echo off the bottom from the side lobe arrives simultaneously with the water column echo in the main lobe, contaminating the data. This results in a loss of data from the last 15% of the water column (Fig. 15e). At Stations 4 and 5, the last 8 to 10 m of the water column were unmeasurable. Unfortunately, this is the area of the water column where the influence of the lateral divergence of the internal tide is thought to be greatest (Shea and Broenkow, 1982). Moreover, no data are obtained in the lower 60 m along the canyon axis where side wall reflections are severe.

Internal Tides in Monterey Submarine Canyon

The second main objective of the study was to further characterize the internal tidal structure at the head of Monterey Canyon. For the observation period described in this work, the internal tide was found to have an amplitude of 70 m. This is within the range of previous measurements of amplitudes between 50 and 120 m (Broenkow and McKain, 1972) and (Shea and Broenkow, 1982). Observations of the internal tides

in Monterey Bay have been made in early spring, late summer, and fall months under conditions of different density stratification. Thus, the large internal tide appears to be a permanent feature at the head of Monterey Canyon. This fact suggests the internal tide is generated locally within the canyon.

A fair amount of evidence supports the possibility of internal tide generation in Monterey Canyon. Cushman-Roisin and Svendsen (1983) explain how the barotropic tide, passing over varying topography, may induce a vertical velocity which displaces the isopycnals in an oscillatory manner. Theoretical work, and model simulations, by Baines (1983) and Prinsenberg *et al.* (1974) suggest that areas of high topographic relief, bumps on the bottom or the walls of canyons, generate internal tides. Further evidence that the internal tide may be locally generated comes from work by Shepard et al. (1979). They interpreted their current meter records in Monterey Canyon in terms of propagating internal waves. Between 384 and 155 m, Shepard found that the waves propagated up-canyon while between 1061 and 1445 m the waves propagated down-canyon. This suggests the waves are generated in the canyon and propagate up and down the canyon from their point of origin.

The large amplitude baroclinic waves found at the head of the canyon may be caused by the interaction of the internal waves with the sloping topography of the canyon. Both Hotchkiss and Wunsch (1982) in Hudson canyon, and Wunsch and Webb (1979) in Hydrographer canyon, found a large increase in internal tide amplitude and energy between the mouth of the canyon and its head. Hotchkiss and Wunsch suggest that canyons

will focus specific frequencies of internal waves depending on the slope of the canyon walls and floor. For a slope, m, they calculated a critical frequency, ω_c, from:

$$\omega_c^2 = (f^2+m^2N^2) \; / \; (m^2+1), \qquad 2$$

where f is the Coriolis parameter, and N is the Brunt-Väisälä frequency. A wave approaching a slope from deep water, whose frequency is less than the critical slope frequency, ω_c, will be reflected back into deep water. Waves with frequencies greater than the critical frequency will be reflected up the slope into shallow water.

A wave will interact with both the sloping walls and floor of the canyon (Fig. 10). For the floor to focus the energy, the frequency of the wave must be greater than the critical frequency. The wave skips up the canyon. If the frequency is less than the critical frequency, the wave is reflected back down the canyon towards the mouth. For the walls, the situation is exactly opposite. The wave frequency must be less than the critical frequency, which reflects the wave back into the canyon towards the bottom. A wave with a frequency greater than the critical frequency will be reflected up the slope and out the top of the canyon. Thus, waves within a finite frequency band will tend to be focused up-canyon and to the bottom. As the waves move into shallow water, small amplitude wave theory predicts the height will increase while the period remains constant. Perhaps more important in MSC, the

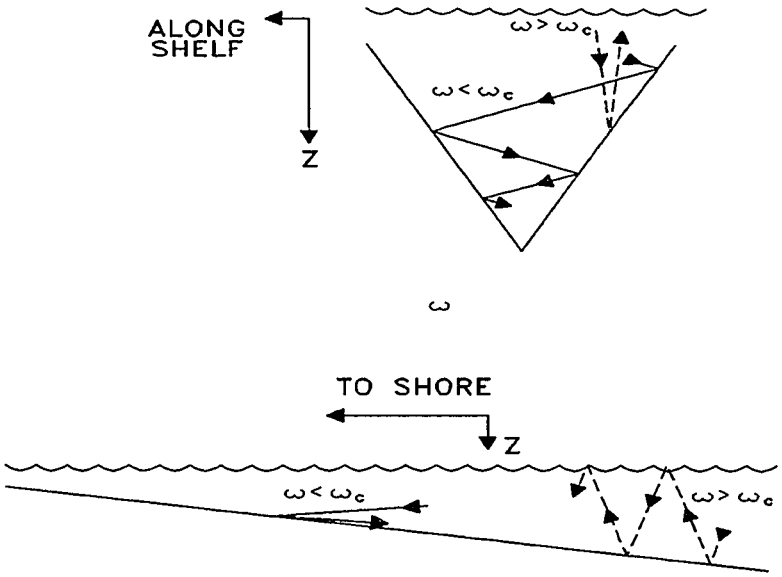

Figure 10. Interactions of a wave of frequency ω with sloping canyon walls and floor of critical frequency ω_c given by Eq. 2 (adapted from Hotchkiss and Wunsch, 1982). In general for $\omega > \omega_c$ the wave will be reflected up the slope and for $\omega < \omega_c$ the wave will be reflected down the slope. The path for a wave $\omega > \omega_c$ is shown by the solid line. The path for a wave $\omega < \omega_c$, is shown by the dotted line.

Upper panel shows the reflection by the canyon walls. Waves less than the critical frequency, are reflected back down the slope, in this case, into the canyon. Waves greater than the critical frequency are reflected up the slope and out of the canyon.

Lower panel shows reflection by the canyon floor. Again, for $\omega < \omega_c$ the waves are reflected back down the slope. For $\omega > \omega_c$, the waves are reflected up slope which is up-canyon. Thus, waves in the frequency band greater than ωc for the floor and less than ω_c for the walls are focused up the canyon and to the floor.

wedge shaped canyon will geometrically focus wave energy below the canyon rim.

Water column mean Brunt-Väisälä frequency, N, which determines the maximum internal wave frequency, over the canyon is approximately 5×10^{-3} rad/sec (Breaker and Broenkow, 1989). From the mouth of Monterey Bay to Moss Landing, the average slope of the canyon floor is on the order of 0.04 and the slope of the wall is 0.12. The local Coriolis parameter is 8.7×10^{-5} rad/sec. This gives a critical frequency, for the canyon floor of 2.1×10^{-4} sec^{-1} and 4.8×10^{-4} sec^{-1} for the walls. The radian frequency of the M_2 tidal constituents is 1.4 x 10-4 sec^{-1} and K_1 is 0.7 x 10-4 sec^{-1}. From these calculations, the walls of the MSC should focus internal waves at M_2 and K_1 frequencies. For the floor, the neither frequency should be focused, although the M_2 frequency is close to the critical frequency. Actual canyon cross sections are V-shaped and Hotchkiss and Wunsch (1982) suggest that the effect from the walls is greater than the floor. Thus, MSC could focus internal waves of tidal frequencies towards the head of the canyon, and this effect should be greater for the M_2 period than the K_1 period.

Results from harmonic regression of the depth variation of the isopycnals support this conclusion (Table 2). The M_2 period amplitudes were 2 to 3 times larger than the K_1 amplitudes. Harmonic regression of surface tidal height produced an M_2 amplitude that was 70% of the K_1 amplitude. Thus, it appears that MSC acts like a filter, selectively

concentrating internal waves at the M_2 period towards the head of the canyon. As the waves enter shallow water their amplitudes become large.

Bottom Currents Due to Internal Tidally Induced Density Flow

The third objective of this study was to attempt to measure the baroclinic increase in bottom currents caused by the internal tide spilling over the edge of Monterey Canyon. Unfortunately, the measurements were not as good as was hoped. This was primarily due to the limitations of the ADCP discussed earlier. Surface speeds were similar to other measurements in the Bay (Breaker and Broenkow, 1989). The mean flow direction for the day-long study was southerly, (Figs. 5, 6, and 7) which occurs only about 35% of the time (Broenkow and Smethie, 1978). Time varying currents were consistent with tidally driven flow steered by bottom topography. The phasing of the M_2 and K_1 constituents was interesting (Figs. 6 and 7). The phase lags suggest a north to south propagation of M_2 constituent and a south to north propagation of the K_1. However, the data set is of insufficient length for a rigorous time series analysis, and I do not feel that statistically significant conclusions regarding phasing between stations can yet be made.

The regression amplitude at Station 4 appeared to increase by 5 cm/s in the deeper part of the profile (Fig. 5). Calculated increases in bottom speeds due to volume divergence range between 2 and 4 cm/sec (Shea and Broenkow, 1982) and 9 cm/sec (Broenkow and McKain, 1972). Those calculations were based on the flow in a 20 m thick bottom layer. The ADCP bin between 29 and 33 m does not sample the deepest 12 m of the

water column, but the increase in near-bottom flow at Station 4 starts about 20 m above the bottom (Fig. 6). Thus, these ADCP measurements support the idea of 20 m thick baroclinic flow across the canyon flanks.

The data at Station 5 were less conclusive. Regression coefficients were not significant for any depths except the surface. This is probably due to a lack of data at Station 5 more than anything else. During the last 12 hours of the study, when stations were occupied for half hour periods, Station 4 was sampled more frequently than Station 5. Another possible problem, is that a small side arm of the canyon is present near Station 5 (Fig. 2). The transect line crossed this tributary canyon. Depth changes here may have induced more current variation or bottom tracking errors in the deeper bins along this run. Also, the internal tide could be spilling out over this lobe, as it does in the main canyon, and interact with the flow from the main lobe. This could seriously complicate the flow regime in there.

The Affect of the Internal Tide on the Current Structure within the Canyon

The last objective of the study was to measure the baroclinic currents within the canyon. The ADCP worked well for this. The current profiles showed a classic two layer flow indicative of internal waves. Figure 8 is similar to many textbook illustrations of two layer flow associated with internal waves (Knauss 1978; Defant, 1961). Pond and Pickard (1983) present a method for describing the horizontal and vertical flow patterns associated with internal waves propagating

diagonally through a continuously stratified water column. The first mode yields a two layer horizontal velocity structure, similar to measurements described here.

On of the most interesting results of this study is that the mean current (as indicated by the harmonic regression) was found to be up-canyon at all depths. Shepard (1974; 1979) observed mean up-canyon flow from most of the current meters deployed in MSC. He sampled at 3 and 30 m above the bottom on each mooring. His records are longer than these here, and showed episodic down-canyon flows among the more common up-canyon flows. Shepard felt that MSC was unique relative to other canyons that he had surveyed in that flow was primarily up-canyon and, moreover, the up-canyon flows were stronger than the down-canyon flows.

One of Shepard's moorings was in 155 m of water near Station 1 in this study. From the current meter 30 m above the bottom, Shepard found the net velocity was 6 cm/s up-canyon, with maximum oscillating speeds of 20 cm/s. Results from 3 m above the bottom showed a net down-canyon flow over the 80-hour record. The average speed was on the order of 8 cm/s with peak oscillatory speeds of 30 cm/s. At the shallow moorings, Shepard states this reversal in mean flow direction occurred frequently. However, he offers little explanation for this phenomenon.
Shepard's shallower current meter at his 155 m station corresponds to the depth of the 125 m bin in the ADCP data here. Harmonic regression results from the ADCP yield a net flow up the canyon of 6 cm/s and amplitude of 17 cm/s. The close agreement between Shepard's and these measurements is surprising, and this agreement lends support to the

notion that ship-born ADCP measurements can yield reliable data (when proper care is taken to correct for ship speed). In addition, the flow pattern observed in this study may be representative of normal flow patterns in the canyon and not a chance occurrence.

A mechanism to drive up-canyon flow has been proposed by several researchers. Nelson *et al.* (1978) suggested that upward flow in the Hudson Valley was caused by an offshore pressure gradient. This pressure gradient occurred during upwelling periods when Ekman transport lead to a build up of water offshore. Freeland and Denman (1983) suggest a similar mechanism for a spur of the Juan de Fuca Canyon. They found the pressure gradients can raise water from a depth of 450 m, whereas winds in the area could only raise water from 250 m.

A second mechanism that could account for up-canyon flow is nonlinear processes associated with internal tidally induced density flow postulated by Shea and Broenkow (1982). As the pycnocline rises above the canyon rim, denser water moves laterally out of the canyon. During the falling tide, some of this water is left behind due to mixing, surface heating and inertia. Since the volume of water left behind must be replaced from deeper down the canyon, a net divergent flow away from the canyon results. Thus, oscillatory motions associated with the internal tide are rectified into a net flow up and out of the canyon. This process causes the canyon to appear as a local upwelling center, bringing cold, deep water near the surface. Bolin and Abbott (1963), and Abbott and Albee (1967), also report lower surface temperatures over the canyon supporting the idea of an upwelling-like

feature over the canyon. However, the flow described here is not wind driven upwelling, a fact noted by both Broenkow and McKain (1972) and Shea and Broenkow (1982).

Data from Broenkow and Smethie (1978) support tidal rectification as the mechanism driving up-canyon flow. They reported low surface temperatures around the canyon head during non-upwelling periods, during which time there was no offshore pressure gradient to drive up-canyon flow. This suggests that, for MSC, the up-canyon flow is "pulled from the head" rather than "pushed from the mouth." They also found evidence of a surface divergence, indicative of upwelling, near the head of the canyon from surface drogues. They calculated an upward velocity of 10 m/day. They felt this number was high, but data from this study suggests that, if anything, 10 m/day may be too low.

Both Broenkow and McKain (1972), and Shea and Broenkow (1982) used volume continuity to calculate the volume of water alternately pumped in and out of the canyon during an internal tidal cycle. Those calculations yielded volumes of 700 x 10^6 m^3 (8 hr^{-1}) and 560 x 10^6 m^3 (6 hr^{-1}). In this study, the spacing between the 25.75 and 26.5 sigma-t surfaces changed by 50 m in 6 hr (Figs. 4 and 11). This requires a lateral divergence of 63 x 10^6 m^3. As noted in Shea (1980) the volume calculations are sensitive to canyon bathymetry and internal wave characteristics. The outer stations in both previous studies were more than 1 km further offshore than Station 1 here (Fig. 1). Thus, the

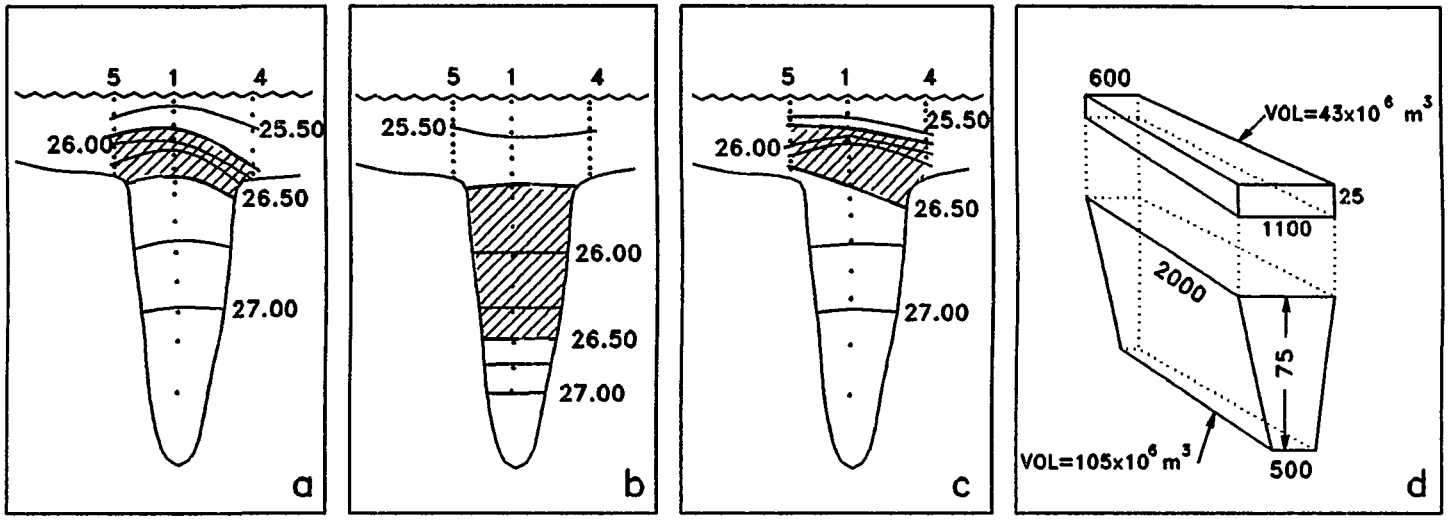

Figure 11. Distribution of sigma-t across Stations 5, 1, 4 during high and low internal tide used in volume divergence calculations. a) High tide at 20:00. Contour interval is 0.25 sigma-t. Depth of the canyon is 185 m. The hatched area shows the area bounded by the 25.75 to 26.5 sigma-t surface. b) Low internal tide at 03:00. c) High internal tide at 09:00. Note the change in size of the hatched area due to the change is isopycnal spacing. These changing areas are used for volume divergence calculation. d) Dimensions and volumes used in volume divergence/convergence calculations. Lengths shown are in meters. Vertical surface areas are based on the hatched areas in panels a-c. The horizontal distance to the head of the canyon was estimated at 2000 m. The difference in volume between the layers of 62×10^6 m^3. This water spreads laterally across the flanks of the canyon and generates current speeds of 4 cm/s out of the sides of the upper box.

surface area of the canyon used for these calculations here is much smaller than in the other studies, leading to the smaller volume divergences. A more comparable calculation is the lateral velocity over the flanks of the canyon generated from the volume convergence and divergence. The volume divergence in this study would result in lateral bottom velocities of about 4 cm/s within a layer 20 m thick. By ADCP measurements, the bottom velocity at Station 4 was greater than 5 cm/s. The ADCP near bottom velocities are similar to the previously discussed speeds calculated by Broenkow and McKain (1972) and Shea and Broenkow (1982). Thus, while the size of the area involved in the calculations varied greatly, the calculated lateral bottom velocities are all similar.

The volume of water rectified during a tidal cycle can be calculated using the mean current profile measured by the ADCP. Since the canyon walls are solid boundaries, any water entering the canyon past Station 1 must either flow back out at another depth or be upwelled out of the canyon. The cross section of the canyon at station 1 was divided into 3 layers. The depths of the layers were selected based on a smoothed profile of mean flow from the harmonic regression (Fig. 12). Velocities below the range of the ADCP were estimated by linearly interpolating through Shepard's (1979) mean speed of 8 cm/s at 152 m. Using speeds of 2.5 cm/s, 4 cm/s and -9 cm/s for the three layers gives a net volume pumped out of the canyon of 44×10^6 m^3 during each 12 hr

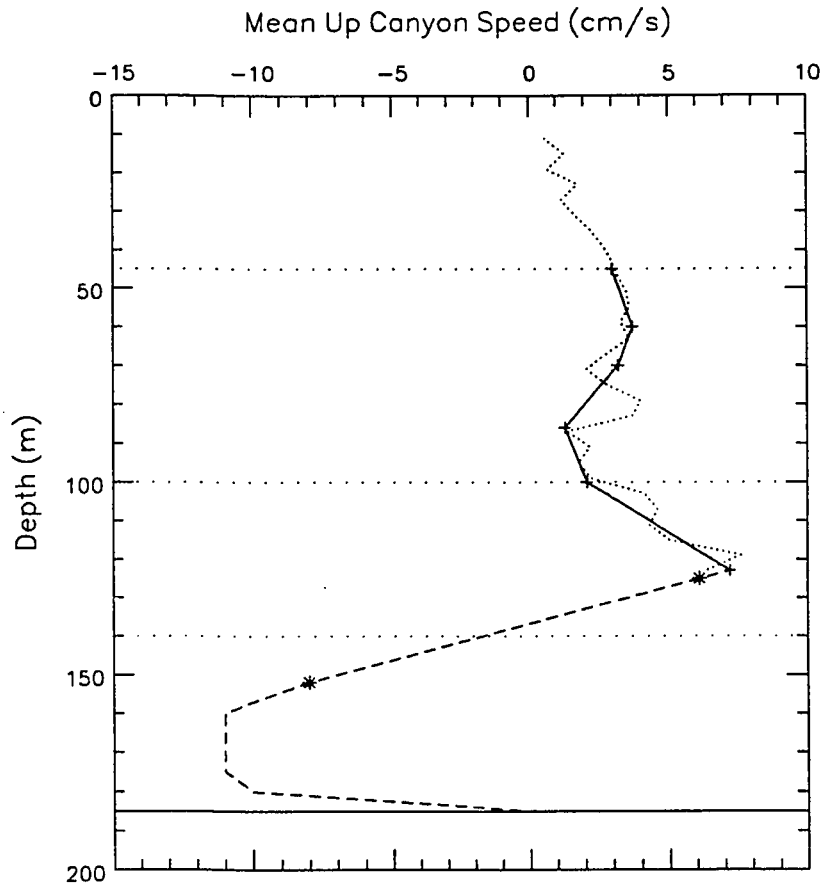

Figure 12. Averaged profile of mean velocity at Station 1 used to calculate vertical velocities in the canyon based on ADCP data and historical data from Shepard (1979). The profile shown by the dotted line is from results of harmonic regressions on ADCP data and is redrawn from Fig. 9. The solid line and + are the visually smoothed version of the mean velocity profile. Points shown by the * are values from Shepard (1979). The dashed line is the interpolated velocity structure through Shepard's data. The horizontal dotted lines show the boundaries of the three layers based on the velocity profile. The canyon rim depth is 45 m and the bottom is 185 m. Speeds in the three layers are 2.5 cm/s in the top layer, 4 cm/s in the middle, and -9 cm/s in the bottom.

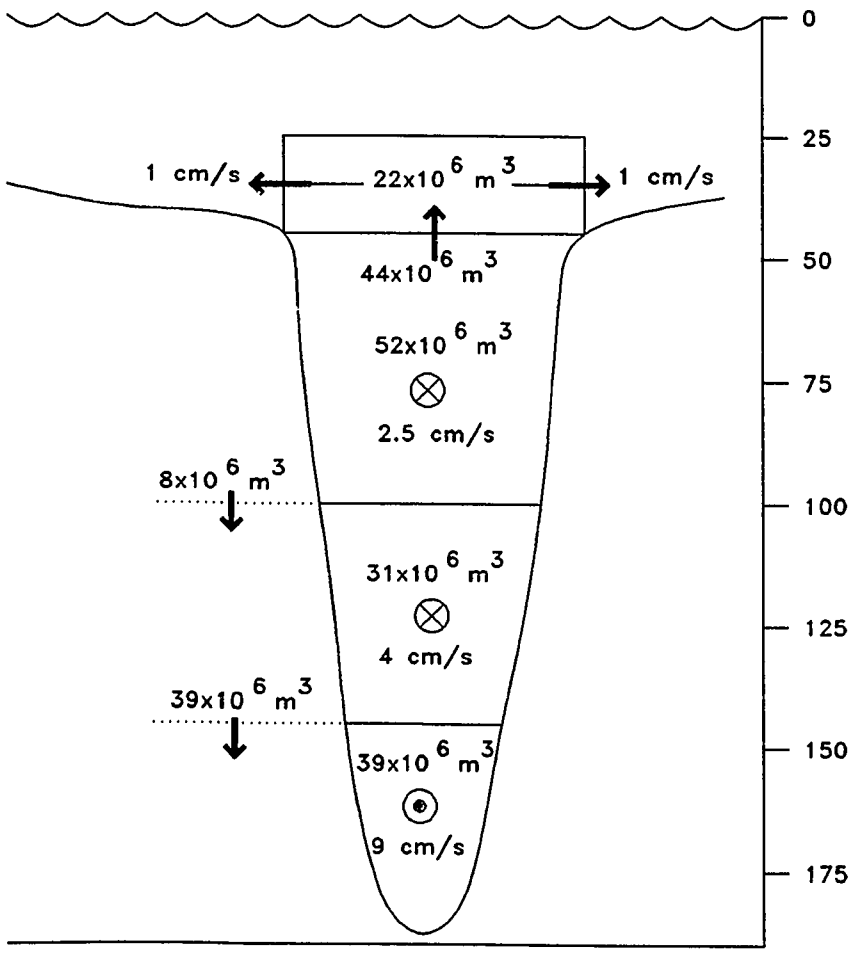

Figure 13. Horizontal and vertical flow model based on the mean flow profile from Fig. 12. Volumes given are for a 12 hour period analogous to the 12 hour tidal cycle. Note the net upward vertical flow. Crosses indicate net up-canyon flow, dot a net down-canyon flow. Canyon geometry was estimated using a triangular cross section for the canyon. Dimensions for the canyon at Station 1 are identical to Fig. 11d. Width of the canyon at the rim is 1100 m and distance to the Head is 2000 m. The net upward volume of 44×10^6 m^3 is 70% of the estimated volume divergence of 62×10^6 m^3.

tidal cycle (Fig. 13). This model results in mean lateral velocities of cm/s across the canyon flanks. The ADCP measurements at Station 4 show a 2 cm/s increase in mean bottom speeds based on the harmonic regressions. Resultant vertical velocities near the canyon are on the order of 50 m/day, which are large compared with the 10 m/day estimated by Broenkow and Smethie (1978). In contrast, Breaker and Mooers (1986) report vertical velocities of 2 m/day from wind driven upwelling off the Central California coast.

Since no direct measurements of bottom speeds in the canyon were made during this study, it is somewhat difficult to estimate flow rate for the bottom layer of the model. It is clear that direct measurements of bottom velocity are needed in future studies since the variation of the velocity in the bottom layer,or any layer, will greatly affect any net divergence calculations. However, if Shepard's (1979) data are indicative of the average flow at 152 m, then 9 to 10 cm/s could be a reasonable estimate. The close agreement between the estimated and measured lateral velocities are further evidence that the modeled flow structure is plausible.

From these calculations the net divergent volume is estimated to be 65 to 70% of the internal tidal volume. Shea and Broenkow (1982), based on CTD casts, estimated the net divergent volume was 50% of the internal tidal volume. The area directly covered by the lateral spreading of this water was thought to be on the order of 26 km^2. They estimated that the nutrient concentration in this volume could contribute up to 30% of the primary production in the northern half of

Monterey Bay. From the close agreement between this and previous studies it is clear that a significant volume of cold, nutrient rich, water is tidally pumped to the near surface. While the results of this process resemble wind driven upwelling, it is important to remember that it is driven by the internal tides and not the wind.

CONCLUSIONS

The internal tide is a permanent feature in Monterey Submarine Canyon. There is indirect evidence to support the generation of the internal tide locally within the canyon. The canyon bathymetry acts to focus internal tides at the M_2 frequency wave towards the head of the canyon, where shoaling and narrowing of the canyon walls cause large amplitudes.

A vessel mounted ADCP was used to directly measure currents, both in the canyon and along the flanks. The ADCP was found to be limited as to how close it could sample to the bottom. Data quality was also sensitive to ship accelerations which were hard to account for in the removal of ship's velocity from the data record.

On the south side of the canyon, the ADCP measured a 5 cm/s increase in velocity within a depth range of 20 to 30 m. This is consistent with the postulated increase in speed calculated by volume continuity in studies by Broenkow and McKain (1972), Shea and Broenkow (1982), as well as in this study.

The velocity structure within the canyon was also measured. The flow in the canyon was oscillatory, with periods corresponding to the M_2 tidal period, and phasing close to the internal tide. The flow was two layered, with the flow in the upper layer flowing opposite to that deeper. This is consistent with the flow patterns associated with internal waves in a continuously stratified water column. The currents in the canyon at all depths measured by the ADCP showed net up-canyon

flow. Note, however, that Shepards (1978) near-bottom current meter showed a net down-canyon flow.

The up-canyon flow measured by the ADCP is most likely caused by the rectification of the oscillatory motions associated with the internal tide. Decreasing isopycnal spacing during a rising internal tide reflect a lateral divergence of water over the flanks of the canyon. Non-linear effects result in a significant portion of this volume remaining behind during the subsequent falling tide. Volume continuity requires replacing this volume with deep water from further down the canyon.

Volume continuity calculations based on the ADCP velocities and observations of Shepard (1979) suggest that 60 to 70% of the volume of water pumped up by the internal tide may be left behind during the subsequent falling tide. This is consistent with calculations by Shea and Broenkow (1992). They suggest that a 50% net divergence could provide nutrients to support, depending on the season, 5 to 30% of the primary production in the norther half of Monterey Bay. Thus the canyon head appears as a local upwelling center. While the effects are similar to those produced by wind driven upwelling, this system is driven by internal tidal pumping and rectification. It is important to note that all of these studies have been limited to a single tidal day. More definitive conclusions concerning the magnitude of this effect must await larger scale, longer term measurements that can be achieved using longer term, multi-ship CTD surveys using several bottom-moored ADCP instruments, or acoustic tomography.

REFERENCES CITED

Abbott, D.P. and R. Albee (1967) Summary of thermal conditions and phytoplankton volumes measured in Monterey Bay, California, 1961-1966. California Cooperative Oceanic Fisheries Investigation Report 11, 155-156.

Baines, P.G. (1973) The generation of internal tides by flat-bump topography. Deep-Sea Research 20, 179-205.

Baines, P.G. (1983) Tidal motion in submarine canyons - A laboratory experiment. Journal of Physical Oceanography 13, 310-328.

Baines, P.G. (1986) Internal tides, internal waves and near-inertial motions. *in* Baroclinic processes on continental shelves. C.N.K. Mooers (Ed.) American Geophysical Union. Washington, D.C. pp. 19-31.

Bolin, R.L. and D.P. Abbott (1963) Studies on the marine climate and phytoplankton of the coast of California 1954-1960. California Cooperative Oceanic Fisheries Investigation Report 9, 23-45.

Breaker, L.C. and C.N.K. Mooers (1986) Oceanic variability off the Central California coast. Progress in Oceanography 17, 61-135.

Breaker, L.C. and W.W. Broenkow (1989) The circulation of an embayment bisected by a major submarine canyon: Monterey Bay. Technical Publication 89-1, Moss Landing Marine Laboratories, Moss Landing, California. 153 pp.

Broenkow, W.W. and S.J. McKain (1972) Tidal oscillations at the head of Monterey Submarine Canyon and their relation to oceanographic sampling and the circulation of water in Monterey Bay. Technical Publication 72-05, Moss Landing Marine Laboratories, Moss Landing, California. 43 pp.

Broenkow, W.W. and W.M. Smethie (1978) Surface circulation and replacement of water in Monterey Bay. Estuarine and Coastal Marine Science 6, 583-603.

Caster, W.A. (1969) Near-bottom currents in Monterey Submarine Canyon and on the adjacent shelf. M.S. Thesis, Naval Postgraduate School, 201 pp.

Cushman-Roisin, B. and H. Svendsen (1983) Internal gravity waves in Sill Fjords: vertical modes, ray theory and comparison with observations. *in* Coastal Oceanography IV(11), H.G. Gade, A. Edwards, H. Svendsen (Eds.) Plenum Press, New York, 373-398.

Defant, A. (1961) Physical Oceanography I. Pergamon Press. New York. 729 pp.

Dooley, J.J. (1968) An investigation of near-bottom currents in the Monterey Submarine Canyon. M.S. Thesis, Naval Postgraduate School, 46 pp.

Freeland, H.J. and K.L. Denman (1982) A topographically controlled upwelling center off southern Vancouver Island. Journal of Marine Research 40(4), 1069-1093.

Gatje, P.H. and D.D. Pizinger (1965) Bottom current measurements in the head of Monterey Submarine Canyon. M.S. Thesis, Naval Postgraduate School, 43 pp.

Hollister, J.E. (1975) Currents in Monterey Submarine Canyon. M.S. Thesis, Naval Postgraduate School, 86 pp.

Hotchkiss, F.S. and C. Wunsch (1982) Internal waves in Hudson Canyon with possible geological implications. Deep-Sea Research 29, 415-442.

Knauss, J.A. (1978) Introduction to Physical Oceanography. Prentice-Hall. Englewood Cliffs, New Jersey. 338 pp.

Martin, B.D. (1964) Monterey Submarine Canyon, California: genesis and relationship to continental geology. Ph.D. Dissertation, University of Southern California, Los Angeles, 249 pp.

Nelson, T.A., P.E. Gadd, and T.L.Clarke (1978) Wind induced current flow in the upper Hudson shelf valley. Journal of Geophysical Research 83, 6073-6082.

Pond, S. and G.L. Pickard (1983) Introductory Dynamical Oceanography. Pergamon Press. New York. 329 pp.

Prinsenberg, S.J., W.L. Wilmot, and M. Rattray (1974) Generation and dissipation of coastal internal tides. Deep-Sea Research 21, 263-281.

RD Instruments (1989) Acoustic doppler current profilers, principles of operation: a practical primer. RD Instruments, 36 pp.

Shea, R.E. and W.W. Broenkow (1982) The role of internal tides in the nutrient enrichment of Monterey Bay, California. Estuarine, Coastal and Shelf Science 15, 57-66.

Shepard, F.P. (1975) Progress of internal waves along submarine coasts, continental margins, and the deep-sea floor. Crane, Russak & Co. New York. 214 pp.

Shepard, F.P. and R.F. Dill (1966) Submarine canyons and other sea valleys. Rand McNally and Company, Chicago.

Shepard, F.P., N.F. Marshall, P.A. McLoughlin, G.G. Sullivan (1979) Currents in submarine canyons. American Association of Petroleum Geologists. Geology Note 8, 173 pp.

Wunsch, C. and S. Webb (1979) The climatology of deep ocean internal waves. Journal of Physical Oceanography 9, 235-243.

APPENDIX

ADCP: Theory of Operation

While a full explanation of the theory and operation of an ADCP is beyond the scope of this thesis, a basic explanation of a vessel mounted ADCP system is provided to assist readers unfamiliar with it. A more thorough description is given by RD Instruments (1989) from which the following is adapted.

The doppler shift is a change in the observed frequency of sound due to relative motion between the source and the observer. For an ADCP this can be written as:

$$F_d = 2\ F_s\ (V/C)\ \cos(A) \qquad 3$$

where: F_d is the doppler shifted frequency, F_s is the original frequency emitted by the ADCP, V is the relative velocity between the source and receiver C is the speed of sound, A is the angle between the relative velocity vector and a line between the source and receiver (Fig. 15a). A factor of 2 is used since the source and receiver are the same.

The ADCP uses measured Doppler shifted echoes from sound scatters in the water column to calculate water velocities. These scatterers are small particles and plankton, and are assumed, on average, to move at the same velocity as the surrounding water. The ADCP underwater unit consists of four transducers, configured in orthogonal pairs and aligned 30 degrees from vertical (Fig. 14). The ADCP emits a sound pulse simultaneously from each transducer. This pulse, or ping, is transmitted at a fixed, precisely known frequency. The frequency of the

ADCP installed on the R/V Point Sur is 150.3 KHz. Sound scatterers in the water column will echo some of the sonic energy back to the transducers. The farther away the scatter is from the transducer the longer it will take for the echo to return. In a process know as range gating, the ADCP divides up the returning echo profile into uniform segments by time (Fig 15b). These segments, or bins, are converted to depth ranges using the speed of sound in seawater. The width of the depth bins and the ping length are set by the user. The manufacture recommends that the ping length be set equal to the bin width, which for a 150 KHz system is 8 m.

The measured Doppler shift occurs along the beam axis. Since the beams are aligned at 30 degrees from vertical, each beam can be resolved into a horizontal and vertical vector component. A pair of beams, such as the pair pointing forward and aft, can be combined to yield a single horizontal and vertical current measurement. The other pair gives the orthogonal horizontal, and a redundant vertical, measurement (Fig. 15c). One of the main requirements for the ADCP to work is that the currents are horizontally homogenous, that is, the measured currents are the same in the four beams (Fig. 15d). The redundant vertical velocity measurements provide a method of checking this assumption, as non-homogeneity results in a large difference between the two vertical velocity measurements.

The two horizontal velocity vectors can be rotated into geographic coordinates if the alignment of the transducers is known. On a ship

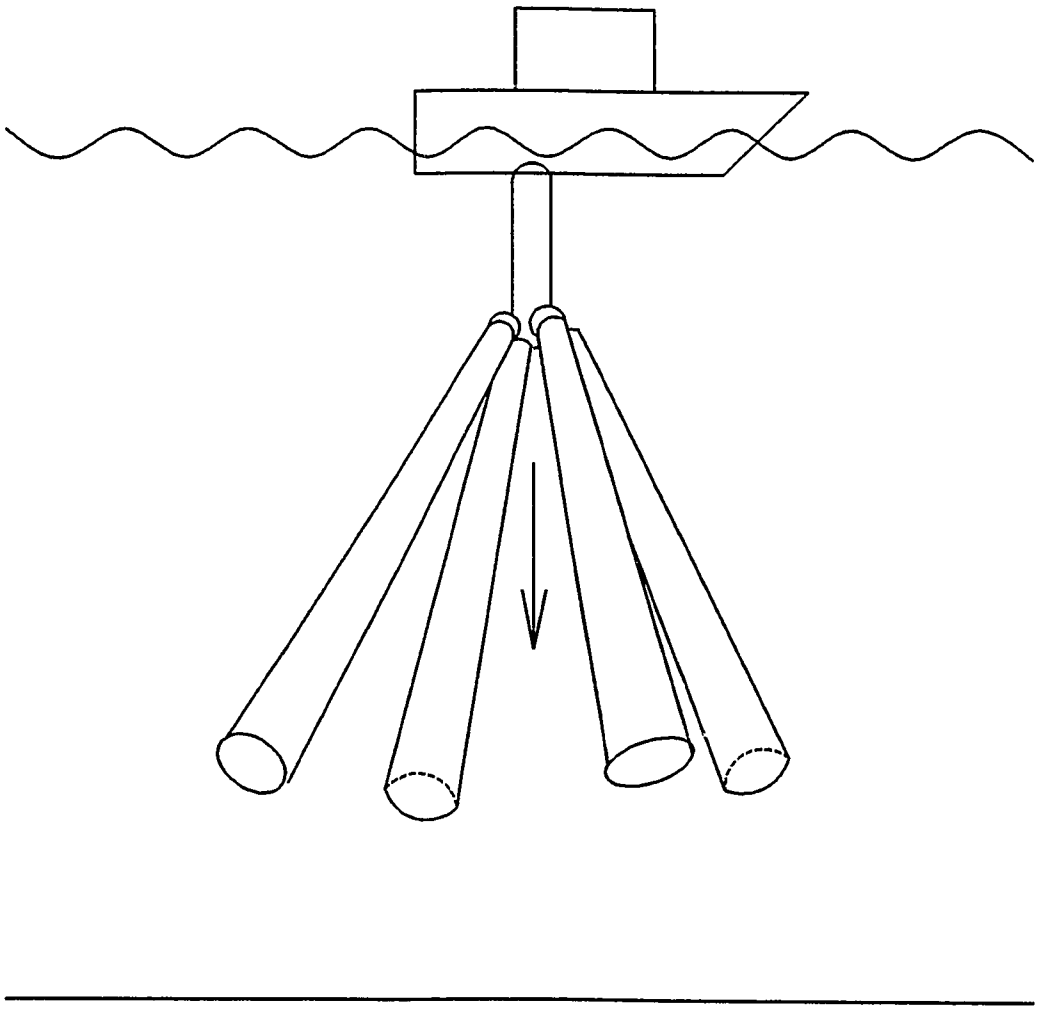

Figure 14. Beam pattern for a vessel mounted ADCP (from RDI, 1989). The angle between beams is 90 deg and the beams are aligned 30 deg from vertical. Normally one beam points in the direction of the bow, one in the direction of the stern, and the other two point to the sides of the ship.

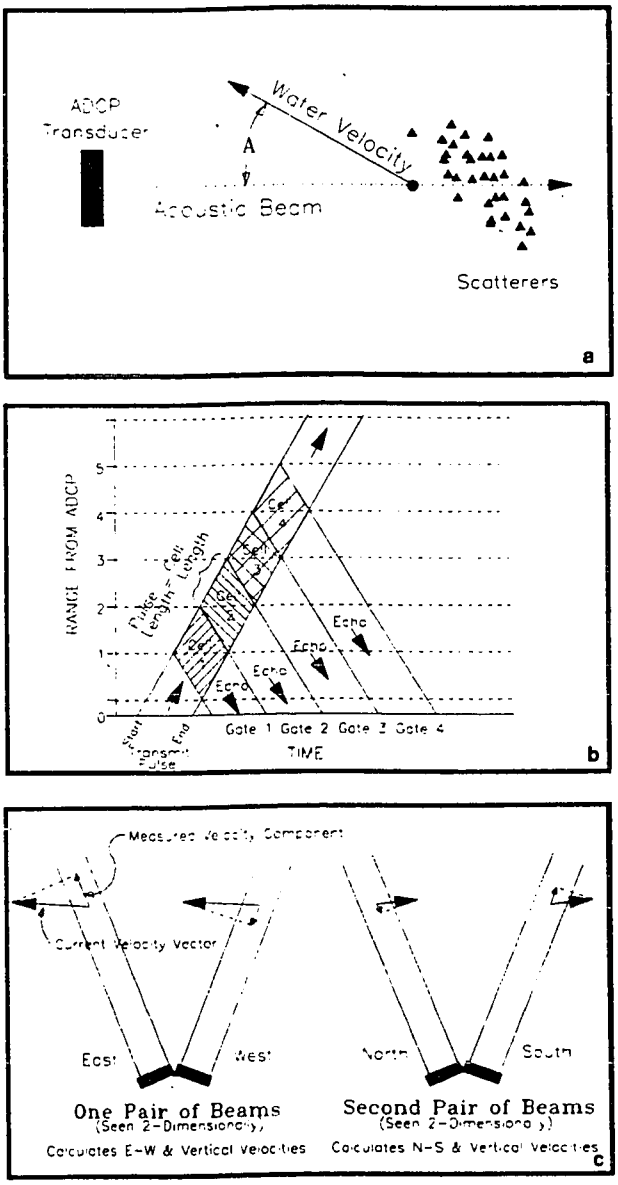

Figure 15. Illustrations of various ADCP parameters (from RDI, 1989). a) Diagram showing definition of the angle A between the acoustic beam and the motion of the scatters used in Eq. 3. b) Diagram showing the concept of range gating. The x axis shows time and the y axis shows sequential ranges from the ADCP. The echos occurring within each range are returned into the sequential bins shown by the numbered gates on the x axis. c) Beam geometry showing how pairs of beams are used to calculate a horizontal and vertical velocity.

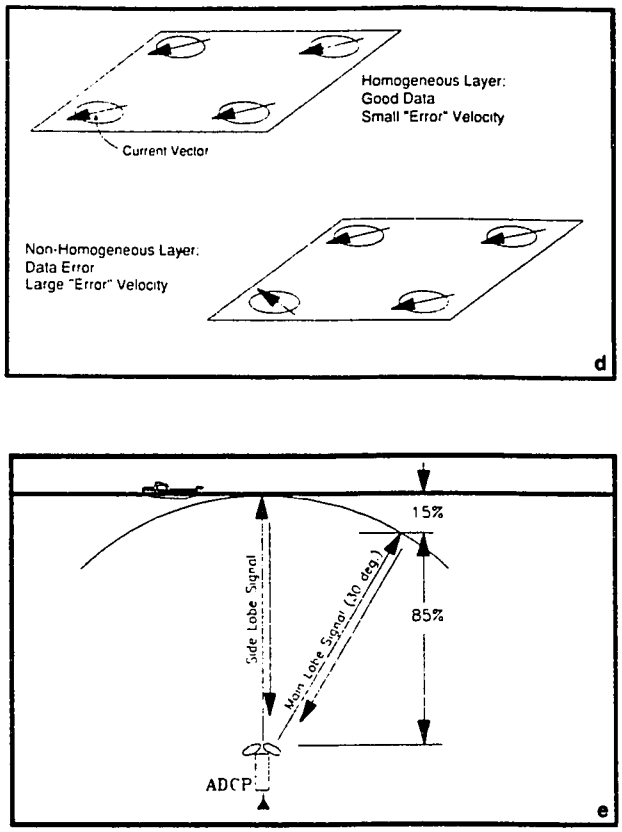

Figure 15. d) Illustration of horizontal homogeneity. The squares show a depth surface intersected by the four beams of the ADCP. For the ADCP to work the currents must be the same with in the area bounded by the four beams as is shown in the upper square. If the currents vary, as in the lower square, the beams cannot be combined to produce the current measurement. e) Diagram showing the geometry of side lobe interaction. The picture shows a bottom mounted ADCP looking up and interacting with the sea surface. The process is identical for a vessel mounted ADCP looking down and interacting with the bottom. Echos from the water column at a range described by the arc arrive at the transduce simultaneously. Data from the main lobe are contaminated by echos from the simultaneously arriving side lobe echos.

this requires knowing the alignment of the transducers relative to the bow of the ship, and the ship's heading. This is generally done by interfacing the ship's gyro compass into the system. Since the Doppler shift is due to relative motion, the velocity vectors at this point contain motion due to water currents and ship motion. As any seasick person will tell you, the motion of a ship is considerable and, to obtain accurate current velocities, those effects must be removed from the record. This is commonly done in one of two ways. The first method of removing ship's motion is bottom tracking. This method only works in shallow water, which is less that 600 m, for the 150 KHz system. To utilize bottom tracking, the ADCP sends out a separate bottom tracking ping. Because the bottom is a strong localized reflector, a longer pulse provides a more accurate measurement of velocity. The echo from the bottom is treated like another depth bin and a velocity from the Doppler shift. Any observed velocity is this bin is due to the ship's motion over the bottom. In deep water ship's speed must be obtained from LORAN or GPS. This method depends on the accuracy of the navigation system and can yield varying results. Resolution of the ships motion is more difficult in practice than described here. And the removal of ship's motion from ADCP records is still the most difficult, time consuming, and error-prone part of the data processing.

The random errors in a velocity measurement from a single ping can vary from a few to 50 cm/s. The magnitude of this error depends on many factors including, transmitted frequency, depth cell size, and beam geometry. Since random errors are uncorrelated from ping to ping,

averaging reduces the standard deviation of the error by the square root of the number of pings. Typically, pings are averaged into 2 to 3 min ensembles. This reduces the random error in the velocity measurements to about 1 cm/s. Errors from other sources such as transducer misalignment, gyrocompass, and estimation of ship's motion all contribute to the overall error. For a typical 150 Khz system, velocity measurement errors, under normal conditions, are thought to be on the order of 2 to 4 cm/s.

The ADCP data acquisition system consists of the transducer array, a deck unit and computer running the Data Acquisition Software (DAS). The deck unit provides power to the transducers, interfaces for gyro compass and computer, and does much of the preliminary signal processing. It provides raw range gated Doppler shifted frequencies from each beam for each ping to the DAS. The DAS averages these pings over an ensemble averaging interval, and calculates velocity for each depth bin for the ensemble. The DAS acquires data from the LORAN or GPS navigation systems. The user configures all of the measurement and sampling interval parameters through the DAS. The DAS also displays raw data and logs it to floppy disks for further analysis. Typical system parameters for a vessel mounted system as installed on the R.V. Point Sur are shown in Table 6.

ADCP technology is still in a high stage of flux. New sources of errors and system problems are being discovered as fast as old problems are solved. Since installation on the R/V Point Sur in 1988 the ADCP

has undergone 3 major firmware changes, 4 software revisions and a major transducer and deck unit upgrade.

Table 6. Typical system parameters for a 150 Khz ADCP as installed on the R/V Point Sur. Profiling range is limited by the acoustic impedance of the water. Velocity errors are primarily related to the reliability of the measurement of vessel motion.

Transmit frequency	150 Khz
Depth profiling range	350 to 450 m
Depth bin size	8 m
Ensemble averaging interval	3 min
Horizontal velocity error	2 to 4 cm/s or greater depending on ship velocity measurement error